A model-based parametric and optimal sizing of a battery/hydrogen storage of a real hybrid microgrid supplying a residential load: Towards island operation

Andrea Monforti Ferrario [a,b,*], Andrea Bartolini [a], Francisca Segura Manzano [c],
Francisco José Vivas [c], Gabriele Comodi [a], Stephen John McPhail [b], José Manuel Andujar [c]

[a] *Università Politecnica delle Marche, Department of Industrial Engineering and Mathematical Sciences (DIISM), Via Brecce Bianche, 60131 Ancona, Italy*
[b] *ENEA, Italian National Agency for New Technologies, Energy and Sustainable Economic Development, C.R. Casaccia, Energy Technologies and Renewable Sources Department, Energy Storage, Batteries and Hydrogen Production & Use Laboratory (TERIN-PSU-ABI). Via Anguillarese, 00123 Rome, Italy*
[c] *Universidad de Huelva; Department of Electronics Engineering, Computer Systems and Automatics, Avenida de las Artes, 21007 Huelva, Spain*

ABSTRACT

In this study the optimal sizing of a hybrid battery/hydrogen Energy Storage System "ESS" is assessed via a model-based parametric analysis in the context of a real hybrid renewable microgrid located in Huelva, Spain, supplying a realtime monitored residential load (3.5 kW; 5.6 MWh/year) in island mode. Four storage configurations (battery-only, H_2-only, hybrid battery priority and hybrid H_2 priority) are assessed under different Energy Management Strategies, analysing system performance parameters such as Loss of Load "LL" (kWh;%), Over Production "OP" (kWh;%), round-trip storage efficiency η_{ESS} (%) and total storage cost (€) depending on the ESS sizing characteristics. A parallel approach to the storage optimal sizing via both multi-dimensional sensitivity analysis and PSO is carried out, in order to address both sub-optimal and optimal regions, respectively. Results show that a hybridised ESS capacity is beneficial from an energy security and efficiency point of view but can represent a substantial additional total cost (between 100 and 300 k€) to the hybrid energy system, especially for the H_2 ESS which presents higher costs. Reaching 100% supply from renewables is challenging and introducing a LL threshold induces a substantial relaxation of the sizing and cost requirements. Increase in battery capacity is more beneficial for the LL abatement while increasing H_2 capacity is more useful to absorb large quantities of excess energy. The optimal design via PSO technique is complemented to the parametric study.

1. Introduction

Increasing shares of Renewable Energy Sources "RES" worldwide have caused an increasing need to address the criticalities related to their variable and non-dispatchable nature [1]. In fact, coupling RES energy to conventional load profiles may prove challenging due to the shift of the temporal profiles of power generation and demand which induces a significant need to oversize the RES capacity. In turn, such oversizing leads to high overproduction and inefficient use of high added-value renewable energy [2]. To takle this issue, distributed Energy Storage Systems "ESS" provide the opportunity to decouple power generation and demand at a local level, allowing the mass grid integration of RES [3] required to achieve decarbonization and climate change mitigation targets [4] without provoking a substantial shock to the existing electrical grid infrastructure [5].

Amongst the available ESS technologies, hybrid configurations such as battery/supercapacitors or battery/hydrogen storage systems have been identified as a promising technological solution in PV powered households to maximize self-consumption and self-sufficiency [6–8]. Battery systems are characterised by low cost and moderate energy density values (up to 150 Wh/kg), together with the capability to operate

at highly variable rate which can be suitable for short-term power dispatching of small energy volumes [9,10]. The main disadvantages of battery storage systems are related to the limited energy capacity of the systems and reduced lifetime, especially under consecutive cycling operation with deep discharge [9,11]. While the coupling of batteries in combination with supercapacitors (power density up to 5 kW/kg) is suitable for short term peak handling, the coupling with hydrogen technologies can be advantageous for medium- to long-term despatch strategies [12] thanks to its high energy mass-based energy content (33 kWh/kg), despite a lower round-trip efficiency (around 35–40%) [13,14].

With the aim of increasing the overall efficiency, reliability and cost in the long-term, hybridised ESS configurations can potentially exploit the advantages of both storage systems used in a complementary way, obtaining a tradeoff between charge/discharge dynamics and suitable stored energy volume for short- and long-term dispatching.

RES-based microgrids with hybrid battery/hydrogen storage at residential scale are a representative and economically feasible test bench for high RES penetration conditions in the large scale [15]. In fact, analysing the power/energy balance at system level allows to understand the impact of different ESS sizing configurations on energy supply security, overproduction, cost, environmental impact and other impor-

* Corresponding author.
E-mail address: a.monforti@pm.univpm.it (A. Monforti Ferrario).

tant performance indicators, which are useful to project in high RES penetration scenarios [16,17].

In addition, PV powered households entail a huge potential impact in terms of emission reduction [18] being representative of the residential sector which today is supplied by grid electricity which presents high Primary Energy Factors and CO_2 emissions [12,19]. In addition, the demand shape of the residential sector is highly variable, characterised by high peak/baseload ratios, which exacerbates the mismatch between RES generation and continuous load supply [20,21].

Based on above, tools for optimal sizing ESS in microgrids play a essential role to guarantee a secure and efficient energy supply, provided at affordable cost.

The main tools and methodologies used for optimal storage sizing in microgrid environments have been comprehensively reviewed by Hosseinalizadeh et al. [22], Erdinc et al. [23] and Abdin et al. [24]. Each ESS sizing configuration is evaluated according to a set of output parameters for energy supply security, efficiency, cost or environmental impact which quantify the performance of a microgrid. According to the specific application requirements or operational criteria, one or more objective functions are determined and the sizing characteristics of the microgrid components are optimized in order to minimize/maximize such objective function.

On the other hand, simulation tools are mainly divided into two categories: (i) aggregate analyses based on efficiency parameters for each component (mainly developed in HOMER) or (ii) model-based analyses where each component is simulated in detail (mainly customly developed in MATLAB/Simulink). The aggregate approach is advantageous in terms of computational effort, reducing the complexity of each analysed case. However, the output results can be somewhat unrealistic from an operational point of view. For example Gangwar [25] and Eltamaly [26] both use an aggregate methodology, which is strongly limited in the assessment of the hourly microgrod perfomance. On the other hand, the model-based approach is much more accurate in terms of operational results – as done by Li et al. [27,28] – and is able to assess different Energy Management Strategies "EMS" [29], although at the cost of higher complexity and computational time is required.

The identification of the optimal values of the ESS sizing characteristics can be achieved with different methodologies. The simplest approach used in literature is by parametric analysis [30,31], where the whole search space is simulated and analysed, finding the optimal solution directly from the simulation of the entire workspace. This approach has the advantage of showing not only the optimal solution but also the variation trends of the selected performance parameters with the variation of the decision variables also for non-optimal regions of the search space, which might be of interest. However, such method is limited to a small amount of variables and presents increased computational burden given the lack of an efficient search method [32].

To address to such limitation, one of the most widespread numeric search algorithm is the Particle Swarm Optimization "PSO" which is characterised by its simplicity of implementation, rapid convergence and high number of input variables which can be potentially processed, which is convenient for optimization problems such as microgrid sizing [23,26,32].

The main research question which this paper aims to answer is *(i)* to identify the optimal sizing configuration and cost of the hybrid battery-hydrogen ESS in a real RES-microgrid which supplies a realtime residential load towards island operation. The paper also contributes to *(ii)* analyse the impact of increasing self-sufficiency ratios of a residential user in terms of storage capacity and cost of the supplying microgrid.

The objectives of the paper are pursued using a detailed component-orientated model-based approach (previously calibrated by the authors with experimental data [33,34]) with four different rule-based EMS whose system performance under fixed storage capacity has been analysed in previous work by the authors [33,35]. The search for the optimal storage configuration (which is the main step forward respect to the previous work of the authors) is carried out with a parallel approach via

a multi-dimensional sensitivity analysis and a PSO algorithm, in order to understand trends between the design variables and performance parameters or to quickly identify the optimal configuration, respectively.

The literature gap consists in the fact that most of the analysed studies either implement only one ESS [31,36] or analyse the impact of one variable at a time [17,26,37,38] or are based on an aggregate approach [39,40]. There are fewer examples of model-based analyses of hybrid battery-hydrogen ESS sizing optimization [27,28,30]. None of the revised papers address the variation of more than one design parameter contemporarily or under different EMS. All the aspects previously listed represent elements of novelty for the proposed paper.

Table 1 provides a brief overview of the analysed literature and details the main contributions of the authors' proposal.

In order to analyse different ESS configurations from an energy capacity point of view (kWh$_{useful}$), the sizing paraemters V_{tank} and Q_{batt} are varied in a wide search space and optimal sizing configurations are searched by applying both parametrical analysis and a Particle Swarm Optimization (PSO) [48] search method, coupled with a model-based simulative approach under 4 energy management strategy scenarios (battery-only, H$_2$-only, hybrid battery priority, hybrid H$_2$ priority). Cost optimal sizing solutions are found and compared for each scenario for decreasing thresholds of Loss of Load "LL" (from 10% to 1% respect to the nominal load energy), in order to analyse the technical and economic performance trends of the system for increasing grid independence, exclusively achieved by local zero-emission renewable energy sources.

2. Materials and methods

In Section 2.1 and 2.2 the case study is described in terms of microgrid topology, component characteristics (Section 2.1) and time-dependant input data – meteorological and demand profile – (Section 2.2). Section 2.3 presents the modelling tools utilized in the present work. The component modelling is only summarized in Section 2.3.1 since it has been taken from previous works by the authors [33,34] which present a full component model analysis for the analysed microgrid based on custom MATLAB code, including empirical validation & error analysis for each specific component. In the same fashion, the system modelling is only briefly mentioned in Section 2.3.2 since the power despatch algorithms are thoroughly described in the previous works [33,35]. For specific details the reader should refer to such previous works.

2.1. Huelva microgrid – configuration

The storage sizing analysis is tailored for the case study of the hybrid renewable microgrid located in Huelva, Southern Spain, whose simplified scheme is illustrated in Fig. 1. The microgrid presents several renewable energy systems at kW-scale which represents a suitable test bench for studying hybrid energy systems. The RES production side (15 kW$_p$ PV panels, 3 kW Wind Turbine "WT") feed power without limitation into the DC bus, according to the available meteorological resources. A hybrid battery-hydrogen ESS (40.8 kWh lead acid battery and a hydrogen loop composed of a 10 kW Alkaline Electrolyser "ALKEL" and PEM Fuel Cell "PEMFC") is installed to absorb and discharge energy from/into the DC bus. Both storage systems can act complementarily according to the implemented EMS despatch algorithm, providing various possibilities in terms of net power management within the microgrid boundaries. The main technical caracteristics of the microgrid components are listed in Table 2.

The microgrid is considered to supply a residential load connected to the AC bus; the power is assumed to be exchanged internally on the DC bus and exchanged with the load (connected in the AC side) via the main inverter. In its present configuration, the microgrid presents a bidirectional grid connection on the AC bus. However, since the scope of this study is to analyse the behaviour of the microgrid towards island operation under different ESS configurations, the resulting energy import

A. Monforti Ferrario, A. Bartolini, F. Segura Manzano et al.

Advances in Applied Energy 3 (2021) 100048

Table 1

Overview and comparison of analysed literature for optimal ESS sizing in hybrid microgrids.

| ref	modelling approach	Advantages	Disadvantages
[25,26,31,39,40]	Aggregate analysis	• Fast modelling of hybrid battery/H₂ systems • Many decision variables analysed	• No detailed hourly operational data • In-built optimization tool (sub-optimal regions not assessed)
[16,27–30,32,33,35,41–47]	Model based Optimization	• Component-orientated • Detailed hourly operational data • Customizable EMS • Advanced optimization tools (Particle Swarm, Genetic Algorithms, MILP, Fuzzy logic)	• Complex modelling environment • High computational burden • Optimization process unrelated to physical components • Experimental data required for model validation
Authors' proposal		• Multi-dimensional sensitivity analysis • Model based 1 & 2-variable analysis (contemporary) • Sub-optimal regions are analysed • PSO algorithm • Fast convergence to optimal configuration	• Multi-dimensional sensitivity analysis • Non-optimal search method → simulate entire search space • Limited amount of analysed variables • PSO algorithm • No information on sub-optimal regions
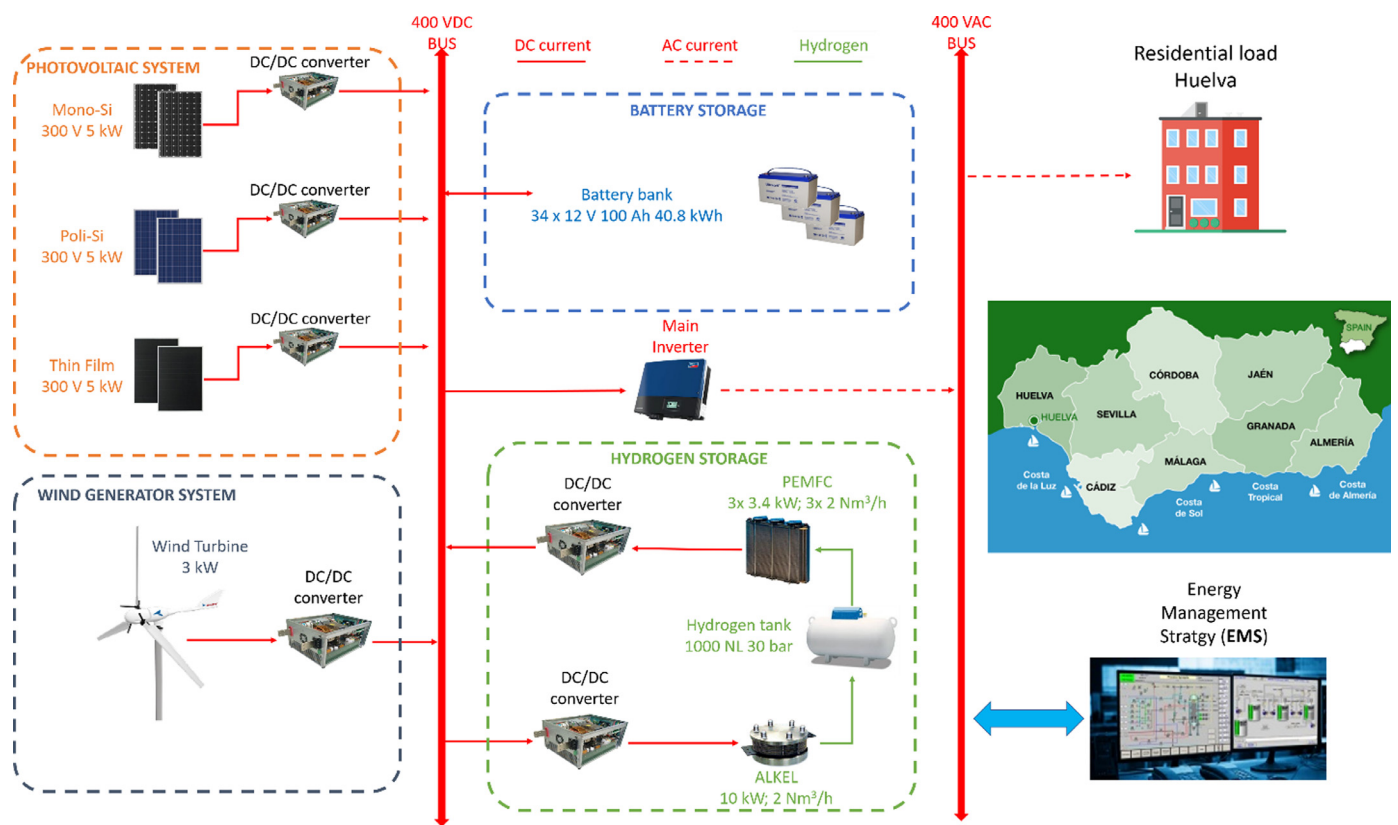
Fig. 1. Hybrid renewable microgrid at University of Huelva.

from the grid represents the Loss of Load and the energy export towards the grid represents the Over Production "OP" from RES generation. In this way the microgrid stand-alone response is simulated, without actually requiring an actual stand-alone operation of the system.

Since the objective of the study is to analyse the performance of the hydrogen ESS in terms of energy capacity rather than charge/discharge dynamics, the systematic variation of the electrolyser and fuel cell rated power values ($P_{el,nom}$, $P_{fc,nom}$) has not been considered. This assumption is justified by the fact that – as shown in Annex I – a variation of such parameters has limited impact on the overall performance parameters (LL, OP, η_{ESS}) in the range between 2 and 10 kW$_{e,nom}$ (especially for the fuel cell, which is the downstream component). Only for very small nominal power values (i.e. ≈1 kW$_{e,nom}$) a significant impact on the performance

parameters is found which, however, is not an area of interest of the search space (proximate to implementing no storage). Furthermore, the variation of the nominal power of the electrochemical systems would undermine the validity of the empirical models used (Table 3) which are calibrated on the base-case nominal power values (10 kW$_{e,nom}$ for both systems), hindering the validity of the obtained results.

2.2. Input data

2.2.1. Meteorological data & analysis

In order to simulate the typical operation of the microgrid and not a specific year, statistical geographic-based meteorological data are implemented.

Table 2
Baseline parameters of the microgrid components.

Component	SupplierModel	Nominal Parameters
PV panels	Isofoton® ISF-250	3×5 kW$_p$
mono/poli/a-Si	Atersa® A-230P	
	Schott® ASI 100	
Wind Turbine (WT)	Enair®	3 kW
	E-30PRO	
Alkaline electrolyzer	Nitidor®	10 kW$_e$
(ALKEL)	Standard line	2 Nm^3$_{H2}$/h
Hydrogen tank	Lapesa®	1 m^3, 30 bar
PEM Fuel Cell	Ballard®	3×3.3 kW$_e$
(PEMFC)	FCgen 1020ACS	3×2 Nm^3$_{H2}$/h
Lead-acid battery bank	U-Power® UP100–12	34×12 V
(BATT)		100 Ah

The meteorological input dataset is obtained from the PV-GIS database [49] which provides TMY P-50 (Typical Meteorological Year with P50 uncertainty rate [50]) datasets in hourly resolution for given geographical coordinates. In particular, Global Horizontal Irradiance "GHI", ambient temperature T$_{amb}$ and W10 (wind speed at 10 m height) data is extracted for the coordinates of Huelva, Spain (Fig. 2). The GHI data is corrected according to the tilt angle of the installed solar panels via the geometrical relationships presented in Maleki et al. [51], while the W10 data is corrected at the actual Hub Height "HH" of the WT (25 m), using a shear factor α equal to 0.3 [52] (Fig. 2).

The solar radiation resource (W/m^2) presents a strongly seasonal and daily trend, peaking around 1000 W/m^2 in daytime summer season which is reduced to around 400 W/m^2 in the winter season, obviously radiation is null in night-time.

The average radiation during the daytime is 355 W/m^2 and the yearly irradiation is around 1.55 MWh/year. Also the ambient temperature follows a similar seasonal trend, with a fairly constant temperature during summer (20–25 °C) and mild temperatures during the winter (10–15 °C), typical of subtropical climates [53]. In contrast, wind speed is fairly low all around the year, presenting a yearly average equal to 4.4 m/s with a slight increase in winter (6.2 m/s during February) afternoons.

2.2.2. Load data & analysis

As previously mentioned the microgrid is analysed considering a real residential load whose data (2019) is obtained by the monitoring of a 100 m^2 residential dwelling of a 12-apartment building, located in Huelva, Spain [53] – Fig. 3. The dwelling consists of a single-family house with an occupancy of 4–5 people with a preferential use during the morning and evening and during winter season. The thermal demands of the dwelling are partly met by supporting electrical com-
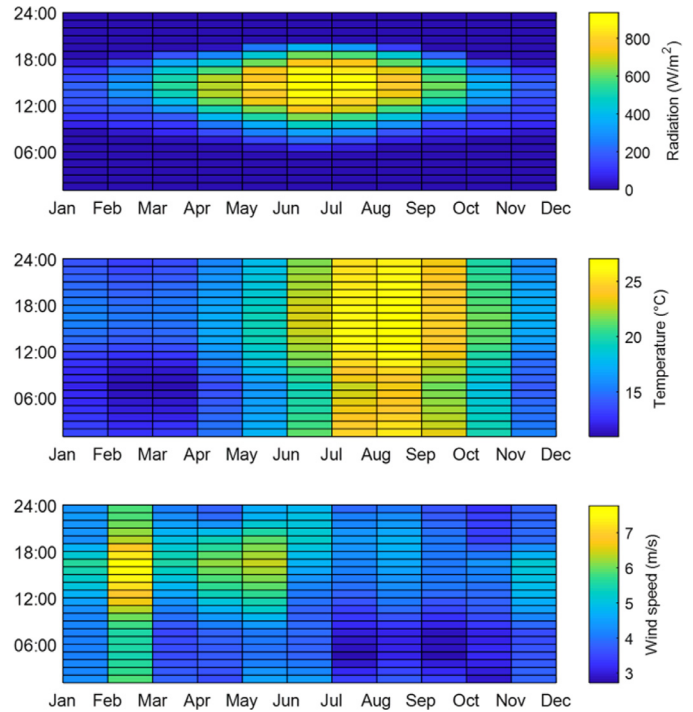

Fig. 2. Yearly heatmap data of (top) solar radiation (tilt angle φ=45°); (middle) ambient temperature; (bottom) wind speed (HH=25 m).

ponents (Air conditioning "A/C", Heater, Domestic Hot Water "DHW" boiler) which mainly operate in electric heating mode during winter, while electric cooling is seldom used due to the advantageous subtropical climate during summer. All the circuits are continuously monitored by voltage and current sensors which send the measured data every 5 s to the data acquisition system specifically developed by the University of Huelva.

The load was resampled to an hourly resolution (1-h average value), in accordance with the modelling timestep (see Section 2.3). The load instantaneous power data (W) shows that the peak electrical consumption is reached in winter (around 3.5 kW), with a reduction of such peak consumption in summer to 1.5–2 kW due to the absence of purely electrical heating. Such kind of heating system is characterised by very high Primary Energy Factor, with respect to other thermal energy technologies (e.g. gas-fired boilers, condensation boilers, electrical heat pumps, geothermal heat pumps, Combined Heat & Power "CHP" units) [12,54]. The baseload of the household is around 150–200 W, fairly constant

Table 3
Summary of microgrid component modelling.

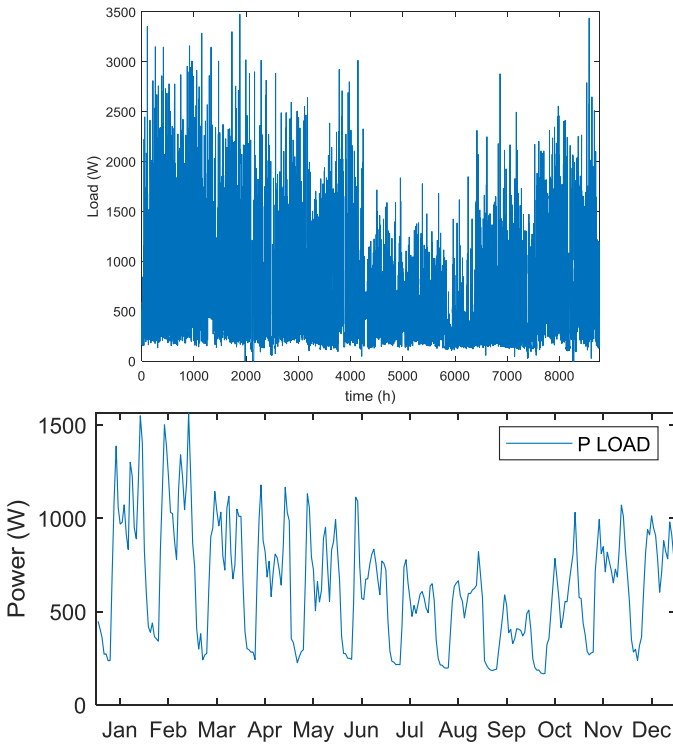| Comp.	Model approach	Main Equations	Eqn.	Ref.
PV	STC correction	$P_{PV} = P_{STC} \frac{G}{G_{STC}} (1 + [\alpha; \beta](T_P - T_{STC})) (1 + \delta \ln(\frac{G}{G_{STC}})^2)$	(1)	[28,58]
WT	Piece-wise power curve	$P_{WT} = 0 \rightarrow V_{HH} < V_{cut-in}$	(2)	[15,59]
		$P_{WT} = f(v_w^3) \rightarrow V_{cut-in} < V_{HH} < V_{nom}$		
		$P_{WT} = P_{WT.nom} \rightarrow V_{nom} < V_{HH} < V_{cut-off}$		
		$P_{WT} = 0 \rightarrow V_{HH} > V_{cut-off}$		
ALKEL	Empirical	I-V polarization curve		[33,34]
		I-P power curve		
PEMFC		$\dot{n}_{H_2} = \eta_F(\frac{N_{cells} I}{zF})$	(3)	[60]
H$_2$ tank	Ideal gas	$pV = nRT$	(4)	[33,46]
		$\Delta p_{tank} = \frac{\Delta nRT}{V_{geom}}$		
BATT	Tremblay (adapted)	$I_{batt} > 0$	(5)	[41,61]
		$V_{batt} = V_{oc} - K \frac{C_n}{SOC + 0.1 C_n} I_{batt} - K \frac{C_n}{C_n - SOC} SOC + A e^{B \cdot SOC} + R_{int} I_{batt}$		
		$I_{batt} < 0$	(6)	[41,61]
		$V_{batt} = V_{oc} - K \frac{C_n}{C_n - SOC} SOC + K I_{batt} \frac{C_n}{C_n - SOC} - A e^{-B \, SOC} + R_{int} I_{batt}$		
		$SOC = SOC_0 - \frac{I_{batt} \, t}{C_n}$	(7)	[33]

A. Monforti Ferrario, A. Bartolini, F. Segura Manzano et al.

Advances in Applied Energy 3 (2021) 100048

Fig. 3. (Top) Monitored yearly total load; (bottom) resampled monthly load – average daily (0–24 h).

Fig. 4. Aggregate monthly energy consumption by circuit.

throughout the year. The contracted capacity is equal to 4.4 kW which is never reached in the analysed data.

In Fig. 3 the average daily resampling (0–24 h) of the load instantaneous power (W) is shown for each month. The daily profiles show typical "M-shape" demand pattern which is typical for residential dwellings, with two evident daily peaks (one in the early morning, one in the evening) related to domestic activities and occupancy, counterbalanced by an intermediate valley period during midday and a baseload profile during nighttime [20,55]. The seasonal trend of the electrical load can also be seen in Fig. 3, showing an overall decrease of the peaks during the summer period due to the absence of electrical cooling during the summer. During summer (June-September), the daily profile is flattened, due to the avoided demand spikes required by the electrical heating appliances (only general purpose appliances). The resampled daily profiles show relatively lower peak values (1.5 kW in January or February vs. up to 3.5 kW seen in the non-resampled yearly data – as seen in Fig. 3), meaning that such peak values are non-recurrent and swamped during the resampling. Although the peak demand values are not statistically significant, they may prove detrimental for the State of Charge "SOC" of the ESS, demanding high currents for limited amounts of time. This aspect highlights the importance of operating with power-based hourly data instead of aggregate energy-based monthly or yearly data, for which such effects are swamped out [47,56]. The resampled baseload power, on the other hand, is fairly constant throughout the year and aligned to the non-resampled yearly data.

The total energy consumption of the dwelling under study is divided into several monitored electrical circuits whose aggregate monthly energy consumption (kWh) is represented in Fig. 4.

The monthly average energy consumption of 466.7 kWh/month and a specific energy consumption of around 55 kWh/m² year classifies the dwelling as Minimum Energy Building "MEB" [57], with a yearly cumulative energy consumption equal to 5.66 MWh/year. The most energy-consuming end circuits result to be the electric boiler for DHW with 34% of the total yearly demand, followed by the general appliances (each around 11–13%) and the electrical heater (12%).
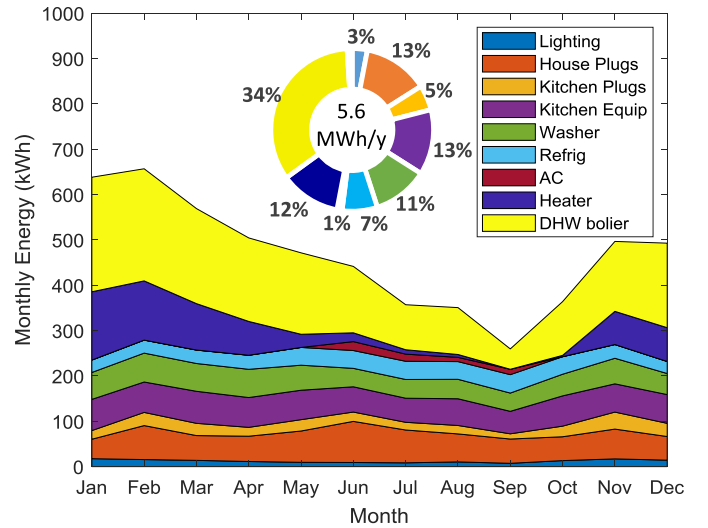
The temporal analysis of the aggregate monthly electricity consumption (Fig. 4) shows a similar behaviour with what discussed for the power data (Fig. 3). A decreasing trend can be observed during summer (up to −35% in August and September respect to the average) with respect to the winter period (with the peak consumption in February with +25% respect to the average). The variations are mainly due to the electrical heating components in winter (heater and DHW support boiler, accounting together for 46% of the yearly electricity consumption), which is not counter-balanced by the cooling equipment in summer which is seldom used (A/C, accounting for only 1% of the yearly electricity consumption). The reduction in energy consumption in summer is also due to the reduced utilization & occupancy of the dwelling by the inhabitants. The trend of the monthly consumptions of the general-purpose loads are rather stable throughout the year.

2.3. Summary of microgrid modelling

As a trade-off between accuracy and computational effort, the system is analysed by means of yearly simulations in hourly timestep in order to focus on the system analysis from an energy standpoint. Each component is simulated according to the specific operating conditions by considering dynamic part-load operation and internal process variables. In Table 3 the modelling approaches, main equations (Equations 1–7) and reference sources are only briefly summarized. As previously mentioned, specific details can be found in previous works by the authors which focus on microgrid component modelling, empirical validation and error analysis [33,34].

The system modelling (Section 2.3.3), developed in Simulink environment, implements a high-level Energy Management Strategy "EMS" approach which is useful to perform long-term simulations, with the objective of analysing the aggregate yearly energy fluxes exchanged by the microgrid. The model calculates the power balance in hourly timestep between the renewable power generation P_{RES} and the demand power P_{load} (according to the hourly meteorological data and load data respectively) on the DC bus as shown in Eq. (8) and assigns net power (P_{net}) setpoints to the ESS according to the implemented EMS logic [29].

$$\sum P_i = 0 \rightarrow P_{net} = P_{RES} - P_{load} \qquad (8)$$

From an energy standpoint, local component control is neglected (although physically it is in place); in fact an hourly timestep is far greater than the characteristic timestep of typical control systems – which is in the order of seconds [62].

The simulations are run in Simulink, setting the standard solver (ode3) for discrete timestep (1 h). The initial values of the ESS must
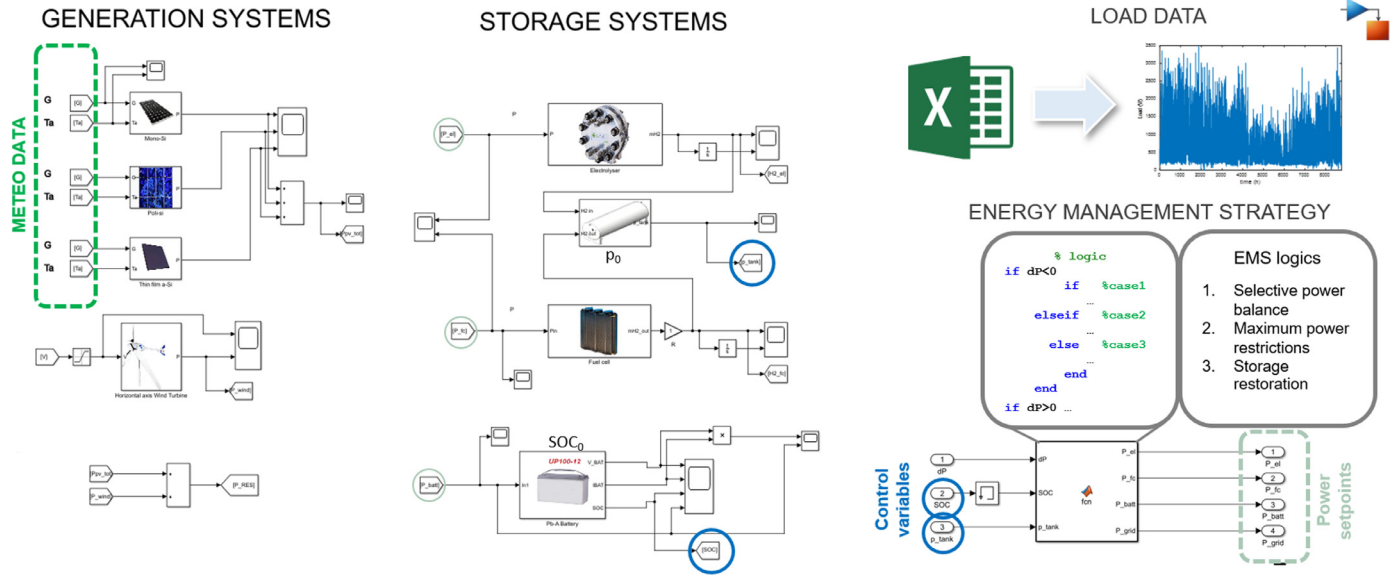
Fig. 5. Global EMS concept scheme.

be initialized, in this case they are set to 50% of each ESS nominal capacity.

2.3.1. Summary of microgrid component models

The PV output power has been simulated as a correction model of the nominal power P_n obtained under Standard Testing Conditions "STC" according to the incident inclined solar radiation at given panel tilt angle and temperature correction coefficients (%/ ˚C) as done by Camps et al. [58] and Li et al. [28].

The wind turbine model follows the implementation of the power curve as a piece-wise function of wind speed evaluated at hub height [15], as done by Feroldi et al. [59]. The wind turbine's operating range is considered between cut-in and cut-off wind speed and constant power operation beyond nominal wind speed.

The electrolyser and fuel cell systems have been modelled by implementing the empirical polarization and power curves obtained from the installed systems in Huelva [33,34] in their typical operation range: in fact, alkaline systems are usually operated at lower power density ranges (0.1–0.8 W/cm^2) [63], respect to PEM systems (0.5–1 W/cm^2) [64] due to the higher conductivity of the electrolyte [63,65].

The produced/consumed hydrogen quantity is directly determined from the stack current by the Faraday law (Equation 3) [60] and is set as input/output to the hydrogen tank. The tank modelling considers hydrogen as an ideal gas, leading to a linear variation of pressure respect to the mass input/output of hydrogen derived from the molar flow [46].

The battery modelling is based on the dynamic battery model proposed by Tremblay [61], adapted by Valverde et al. [41] with decoupled relationships for charge & discharge voltage in function of current and SOC. The model was calibrated based on cyclic charge/discharge data (C-rate within −5 and 5, no limitation in SOC) of a single lead-acid battery unit of the same type of the battery bank.

2.3.2. Summary of energy management strategy algorithms

Once the power balance (Eq. (8)) is calculated for each timestep P_{net} is managed by a case-structured logical algorithm [66] which assigns power (W) setpoints for each timestep to the ESS components in each analysed scenario – see Fig. 5. The component models elaborate the provided power setpoints, determining the new state of the components' internal variables for each timestep.

For the single component ESS scenarios the despatch algorithm is trivial since all the net power is dispatched to the ESS until it is available. For the hybrid ESS scenario two previously developed EMS state
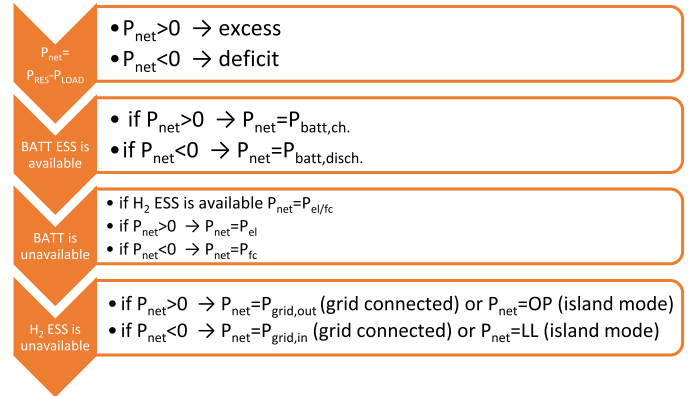

Fig. 6. Battery-priority EMS logical scheme.

control based despatch algorithms are implemented [33,35]: i) battery priority EMS and ii) H_2 priority EMS. The logical structure of the EMS is done by checking the storage control parameters – the battery SOC and H_2 tank pressure p_{tank} – are within the admissible range [SOC_{min}; SOC_{max}; $p_{tank,min}$; $p_{tank,max}$]. Considering the pre-established priority, it will be the battery bank (battery-priority) or hydrogen system (hydrogen-priority) which guarantees the power balance in the first and second instance. Ultimately, if both storage systems are unavailable, the net power cannot be provided/used resulting in unmet load ($P_{net}<0$) or excess electricity ($P_{net}>0$) due to the considered island operation mode. In Fig. 6 and Fig. 7 the two implemented EMS logical schemes are illustrated.

In Table 4 the limits for the storage control parameters are reported. In particular, the SOC thresholds (20%–80%) for the battery bank are chosen to limit deep discharge, which is significantly affects the battery bank lifetime [67]. On the other hand, the hydrogen tank pressure can vary in the whole operating range (from atmospheric pressure, up to the nominal pressure of the vessel equal to 30 bar) without physical limitations.

A hysteresis bandwidth is defined for which as soon as an ESS becomes unavailable due to having reached either the lower or upper limit of the control parameter range, the ESS will remain unavailable until the restoration limit [SOC_{low}; SOC_{high}; $p_{tank,low}$; $p_{tank,high}$] is reached. For ex-
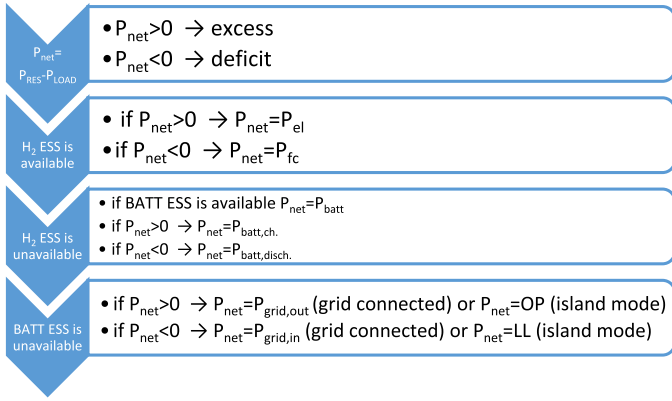
Fig. 7. Hydrogen-priority EMS logical scheme.

Table 4
EMS control parameters.

Parameter	Unit	Value
Correct operation limits [33,35,67]		
$P_{tank,min}$	bar	1
$P_{tank,max}$	bar	30
SOC_{min}	%	20
SOC_{max}	%	80
Hysteresis limits (bandwidth 10 bar; 10% SOC) [68]		
$P_{tank,low}$	bar	10
$P_{tank,high}$	bar	20
SOC_{low}	%	30
SOC_{high}	%	70
Power threshold limits [27,46]		
$P_{el,max}$	$P_{el,nom}$	
$P_{fc,max}$	$P_{fc,nom}$	
C_{max}	5C	

ample, if the battery is discharged below 20% of the SOC, the battery will only allow charging mode until having reached the hysteresis SOC limit of 30%, before being able to discharge again. Hysteresis bandwidth is implemented in order to avoid continuous on/off situations in case of ESS unavailability, which could oscillate around the control variable limit indefinitely. Also, when an ESS is unavailable or within the hysteresis bandwidth, the restoration of such ESS becomes automatically prioritized with respect to normal operation – with the aim to always operate with the two complementary ESSs available (otherwise the hybrid scenario would rapidly fall into either battery-only or H_2-only scenario).

The amplitude of the hysteresis bandwidth affects the promptness of the ESS to return into operation after being unavailable [68]. The chosen hysteresis bandwidth values (equal to 10 bar & 10% SOC) have been selected based on previous experience in similar simulative environments (in terms of system configuration and storage capacities) [33,35] as a trade-off between providing a wide operation range and avoiding unsuitable operating conditions.

Finally, maximum power thresholds (defined in Table 4) are implemented in order to limit the maximum power that each component can physically process [27,46].

3. Energy storage scenarios

The microgrid energy storage configuration is simulated in four scenarios: (*i*) battery-only, (*ii*) H_2-only, (*iii*) hybrid battery priority and (*iv*) hybrid H_2 priority. While for the single component scenarios P_{net} can only be dispatched to the installed ESS in the hybrid scenario P_{net} is dispatched according to the implemented EMS.

The ESS sizing characteristics variation envelope (Table 5) has been selected in order to assess a comparable useful stored energy range of 0–350 kWh (considering the DC bus nominal voltage of 400 V, standard

Table 5
ESS sizing characteristics variation envelope.

ESS variable	Battery-only	H_2-only	Hybrid battery-H_2
Q_{batt} (Ah)	50–1000	0	50–1000
V_{tank} (m^3)	0	0.5–10	0.5–10

H_2 density of 0.0898 kg/Nm^3 and LHV_{H2} equal to 33.33 kWh/kg), net of the nominal round-trip efficiency of the components at nominal conditions, assessed as 85% for the battery (round-trip) [45], 75% for the electrolyser and 50% for the fuel cell [69]. The capacity of the hydrogen ESS is varied with the geometrical volume V_{tank} (m^3) of the tank while the battery ESS is varied by the battery nominal capacity, Q_{batt} (Ah), in order to maintain the voltage of the DC bus fixed to the design value of 400 V_{dc}. In fact, the battery bank voltage directly defines the DC bus voltage since the batteries are directly connected to the busbar (Fig. 1).

The parametric variation of the ESS sizing characteristics is evaluated by the Loss of Load and Over Production performance parameters and their percentages ($LL_\%$ and $OP_\%$) as defined in Eq. (9) and Equation 10:

$$\begin{cases} LL = E_{grid,in} \rightarrow island\ operation \\ LL_\% = \dfrac{LL}{E_{load,nom}} \end{cases} \quad (9)$$

$$\begin{cases} OP = E_{grid,out} \rightarrow island\ operation \\ OP_\% = \dfrac{OP}{E_{PV}+E_{WT}} = \dfrac{OP}{E_{RES}} \end{cases} \quad (10)$$

where E_i is the cumulative yearly energy (kWh) –integration of the instantaneous power in time – related to each analysed component i.

The LL parameter represents the portion of the nominal load energy $E_{load,nom}$ that the microgrid system is not able to supply and is supplied by the grid $E_{grid,in}$ in grid connected mode. The nominal load energy $E_{load,nom}$ is considered fixed equal to the sum of the load demand, even in the case the unmet energy LL is not equal to zero. On the other hand, the OP parameter represents the amount of energy produced by the RES systems $E_{PV} + E_{WT}$, which is not used in the system and injected back into the grid, $E_{grid,out}$.

An overall storage efficiency parameter η_{ESS} is defined as the ratio between the useful energy discharged by the ESS, $E_{out,ESS}$ and the energy initially stored into the ESS, $E_{in,ESS}$ as shown in Equation 11.

$$\eta_{ESS} = \frac{E_{out,ESS}}{E_{in,ESS}} \quad (11)$$

The general objective for this study is to optimize the operation of the microgrid in island mode, therefore minimizing LL and increasing the overall energy supply security of the microgrid [17]. Minimization of OP is only preferable (but in this specific case not of primary importance) in order to enhance the rational use of renewable energy, avoiding that the excess energy is sent to the grid with minimal valorisation or curtailed. Each energy storage scenario is assessed by running parallel Simulink simulations in each ESS configuration with parametric variation of each sizing parameter (Q_{batt} and V_{tank}) within the range reported in Table 5, with a variation step of 10 Ah and 0.5 m^3, respectively.

A sensitivity analysis of the electrolyser and fuel cell nominal power values $P_{el,nom}$ and $P_{fc,nom}$ in a range of 1–10 kW$_{e,nom}$ is provided in Annex I.

3.1. Preliminary economic analysis and cost optimization for target $LL_\%$ thresholds

Although increasing the size of ESS is always beneficial from an energy security point of view (reducing LL and OP for unbalanced energy systems), the increase in cost with size should be analysed [15]. In Table 6, the main economic parameters of the ESS are summarized to assess the cost (CAPEX, replacement & OPEX) of different ESS configurations over the time horizon of 20 years. In particular O&M cost

A. Monforti Ferrario, A. Bartolini, F. Segura Manzano et al.

Advances in Applied Energy 3 (2021) 100048

Table 6
Economic parameters.

Component	CAPEX	O&M	Lifetime	Ref.
Equipment				
ALKEL	1500 €/kW	5%$_{CAPEX}$/y	10 y	[13,72]
H$_2$ tank	2000 €/kg	2%$_{CAPEX}$/y	20 y	[13,72,73]
PEMFC	1500 €/kW	5%$_{CAPEX}$/y	10 y	[13,72]
BATT	200 €/kWh	5%$_{CAPEX}$/y	10 y	[72,74]
Energy cost				
Tariff		€/kWh	Ref.	
LL penalty		8.7	[28,32,70,71]	
OP remuneration		0		

is given as annual rate in percentage function of CAPEX and the component lifetime determines the replacement frequency. Replacement of components is considered at full CAPEX, which is a conservative assumption since most balance of plant components present longer lifetimes. No financial cost is considered due to the small-scale of the energy system which does not imply a financial structure.

For the H$_2$ ESS, not only the tank cost is considered but also the electrolyser and fuel cell costs, since these components are an integral part of the ESS. However, since the electrolyser and fuel cell nominal power are fixed, the electrolyser and fuel cell costs behave as a constant summed to the tank cost.

Due to island configuration, unmet load energy is penalised at the Value of Lost Load "VoLL" – equal to the customer dissatisfaction. Compared to standard electricity acquisition costs (0.136 €/kWh) reported in standard grid connected configurations [34], VoLL is significantly more expensive. Shivakumar et al. [70] have mapped the VoLL for EU countries, reporting for Spain a VoLL equal to 8.70 €/kWh which is confirmed by Kaviani [32] and Schröder [71], which state a VoLL within the range of 2–12 €/kWh for domestic users. Considering the island operation, excess electricity is considered to be curtailed at zero value with respect to reported selling prices (0.030 €/kWh [34]) preventing potential revenue streams.

3.2. Optimal design strategy

The cost optimization module is run on the basis of the energy simulation results, in order to assess the optimal storage sizing and cost for decreasing LL$_{\%}$ thresholds (equal to 10%, 5% and 1%), towards full island operation (LL$_{\%}$ equal to 0%, i.e. fully self-sufficient RES based microgrid).

The optimal design of the ESS is assessed as a two-variable function of the storage capacities of the two ESS systems (Q$_{batt}$ and V$_{tank}$, as previously discussed). The objective of the optimization process is to identify the configuration that yields the least total storage cost C$_{tot,ESS}$ (Eq. (12)), which includes: *i)* the total CAPEX cost of the systems (Eq. (13)) calculated respect to the storage capacities; ii) the replacement cost C$_{replace}$ (Eq. (14)) of each system according to the component lifetime respect to the analysed time horizon (20 years); *iii)* the OPEX cost C$_{OPEX,ESS}$ including O&M cost and penalisation cost for LL (Eq. (15)). The cost equations which compose the cost objective function to be minimized are the following:

$$C_{tot,ESS} = C_{CAPEX,ESS} + C_{replace} + C_{OPEX,ESS}\, n_{tot} \tag{12}$$

$$C_{CAPEX,ESS} = C_{batt} + C_{tank} + C_{ALKEL} + C_{PEMFC} =$$
$$= Q_{batt}c_{batt} + V_{tank}\, c_{tank} + C_{ALKEL} + C_{PEMFC} \tag{13}$$

$$\begin{cases} n_{replace} = n_{tot}/n_{lifetime} \\ C_{replace,ESS} = C_{CAPEX,ESS}\, n_{replace} \end{cases} \tag{14}$$

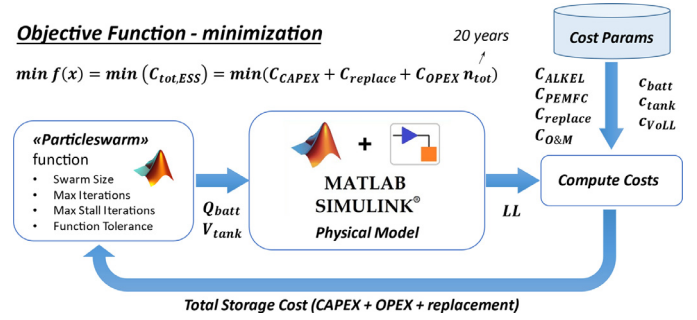$$C_{OPEX,ESS} = C_{O\&M} + LL\, c_{VoLL} \tag{15}$$

Fig. 8. Scheme of the PSO optimization process.

Where c_{batt} and c_{tank} represent the specific costs reported in Table 6; $n_{replace}$ is the number of replacements during the time horizon n_{tot} (years), respect to the lifetime of each component $n_{lifetime}$ (years); $C_{O\&M}$ is the annual operations & maintenance cost of each system given in Table 6 and c_{VoLL} is the penalisation cost for the LL, equal to the value of lost load (€/kWh).

With the parametric analysis the whole search space is simulated (2000 possible configurations considering the design variables range and variation step), the optimal configuration for each LL$_{\%}$ threshold is found by extracting the minimum cost configuration of all the cases within $a \pm 0.5\%$ range of the desired threshold.

In order to improve such search process, a constrained PSO algorithm has been implemented to search the cost-optimal configuration. The implementation of the PSO algorithm is done in MATLAB environment using the "*particleswarm*" function [75]. The settings of the PSO algorithm and its stopping criterions are reported in Table 7. Following the PSO algorithm the function iteratively searches through the given ranges of the design variables and passes them as parameters to the Simulink model. The simulation is executed and through Eqs. (12) to 15 the total storage cost of the simulated configuration is computed. The logical flowchart of the data exchange between the optimization code and the Simulink model is shown graphically in Fig. 8. The search continues until one of the stopping criteria is met, for which a number of consecutive solutions do not show a significant decrease in total storage cost. A virtual constraint is enforced by applying a very high negative cost externality on the objective function (Eq. (12)) for every kWh of LL that exceeds a predefined threshold (the maximum allowable LL$_{\%}$).

4. Results and discussion

The numerical results of the simulations are presented and discussed in this section. Section 4.1.1 reports the results of the single-components storage scenarios. For the hybrid battery-H$_2$ scenarios the results are represented as parametrical 2-variable functions for both EMS in the following Sections 4.1.2 and 4.1.3. Finally Section 4.2 shows the results of the preliminary cost optimization process, considering the preliminary economic analysis parameters discussed in Section 3.1.

Fig. 9 shows the overall energy and power balance between the generation and the load without any ESS in place. In the energy balance, it can be observed that the PV production is predominant (producing between 50% to 95% of the monthly energy in winter and summer respectively) respect to the WT given the favourable solar radiation conditions in Southern Spain. The PV production results strongly oversized respect to the load, the overproduction during spring/summer (March to September) is 2–5 times the monthly energy demand. Similar results are found in literature at comparable latitudes [2,15,30] in energy systems characterised by high predominance of PV . Also the shape and peak/baseload ratio result critical for the energy balance [38] inducing a significant time-shift (0–24 h average resampling) between the load (especially in the morning and evening) and the generation (predominantly PV in solar hours), especially in winter periods (November-

A. Monforti Ferrario, A. Bartolini, F. Segura Manzano et al.

Advances in Applied Energy 3 (2021) 100048

Table 7

Particleswarm function settings – rest default.

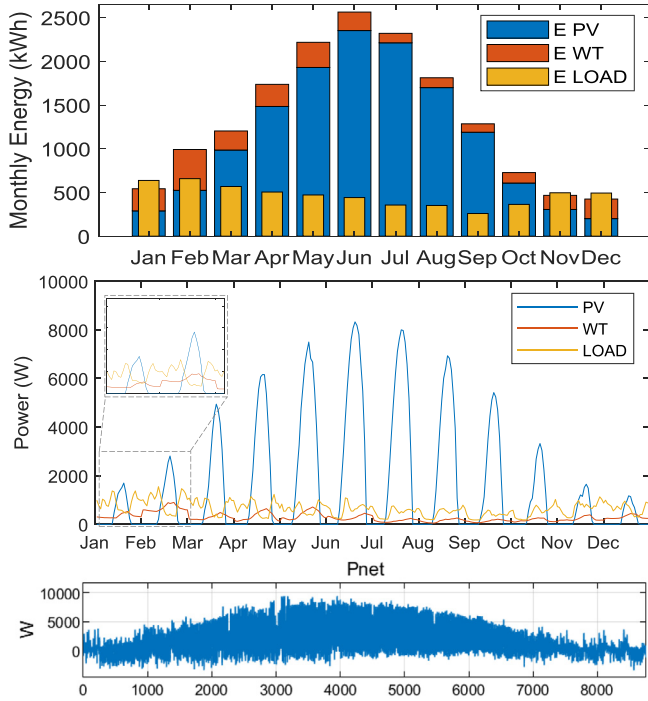| Parameter	Value	Description
Swarm Size	25	Number of particles in the swarm
Max Iterations	150	Maximum number of iterations for the whole swarm
Max Stall Iterations	10	Number of consecutive last iterations with objective change less than tolerance
Function Tolerance	5 e-4	Maximum objective change admissible over the last Max Stall Iterations

Fig. 9. (Top) Monthly energy balance; (middle) average daily power balance resampling (0–24 h) by month between generation and load; (bottom) yearly net power exchanged by the ESS.

March) due to electrical heating, requiring an ESS to manage the net power.

4.1. Baseline simulations

The simulation results of the battery-only (Q_{batt}=100 Ah; V_{tank}=0 m^3) and hydrogen-only (Q_{batt}=0 Ah; V_{tank}=1 m^3) baseline scenarios are shown in Figs. 10 and 11. It can be observed that the control parameters (p_{tank} and SOC) are successfully controlled within the defined operational range by the EMS. The system – for both simulated ESS – enters a deficit phase during autumn/winter (the first and last 1000–2000 h, where the peaks of demand are highest both in average and in maximum value) where the ESS is discharged and grid support is required despite the overall oversizing of the RES and ESS systems respect to the load. Also the time-shift effect (previously described) between RES production and the evening peak of demand is detrimental for the LL. During summer (2000<h<6500, with minimum demand and increased solar radiation) the energy balance is strongly dominated by PV overproduction and the ESS is saturated to the upper limit; during this period excess energy is abundant.

The baseline hybrid battery-hydrogen scenario (Q_{batt}=100 Ah; V_{tank}=1 m^3) simulation results under the two EMS (Figs. 12 and 13) are similar to those reported and discussed in Monforti et al. [33] and Vivas et al. [35] (simulated under a slightly different load condition), showing a clear oversaturation period of both ESS period during summer (March to September) and limited deficit periods in winter. The effect

Table 8

Baseline simulation results.

Scenario	Battery-only	H$_2$-only	Hybrid battery-H$_2$ EMS Battery-priority	H$_2$-priority
E_{el} (MWh)	0	4.970	0.662	4.959
E_{fc} (MWh)	0	1.812	0.266	1.808
$E_{batt,ch.}$ (MWh)	2.789	0	2.399	0.069
$E_{batt,disch.}$ (MWh)	2.149	0	1.806	0.059
OP (MWh)	10.415	8.233	10.142	8.186
LL (MWh)	0.481	0.741	0.404	0.675
E_{RES} (MWh)	16.252	16.252	16.252	16.252
$E_{load,nom}$ (MWh)	5.601	5.601	5.601	5.601
Performance parameters				
$LL_\%$ (%)	8.59%	13.22%	7.22%	12.06%
$OP_\%$ (%)	64.40%	50.66%	62.08%	50.37%
$\eta_{storage}$ (%)	75.10%	36.14%	66.21%	36.94%

of the ESS prioritization can be clearly seen: in the first case most of the energy is processed by the batteries, inducing a stronger variability of the SOC with respect to p_{tank}; the opposite happens for the second case in virtue of the implemented EMS [29,76].

All the baseline simulation results are collected in Table 8, including the cumulative energy for each component E_i and the main performance parameters.

The increased use of hydrogen generally decreases the overall storage efficiency (η_{ESS} as low as 34–35% in H$_2$-predominant simulations and around 50% in the hybrid battery-priority simulation) due to lower nominal efficiency of hydrogen systems [29,33]. The $LL_\%$ increases and the $OP_\%$ decreases since a larger volume of energy is converted by electrolysis, which is a highly energivorous process (around 5 MWh/year absorbed by the electrolyser against only 2.5–3 MWh/year charged into the battery) [77]. However, a larger portion of such energy volume is converted into losses, according to the lower storage efficiency [31,45]. Instead, the use of batteries increases the storage efficiency (up to 75% in the battery-only simulation thanks to the higher nominal efficiency), decreases the $LL_\%$ (down to 7–8%) and increases $OP_\%$ (above 60%).

The unmet load is relatively low (in the order of 400–700 kWh/year) compared to the excess energy (between 8 and 10 MWh/year), caused by the summer PV overproduction (E_{RES} equal to 16.25 MWh/year, constant for all scenarios) which leads to high values of $OP_\%$ (between 50 and 65%) for all scenarios. High $OP_\%$ conditions are frequently reported in other literature works, due to high RES penetration and down-sizing of the ESS [2,15,30].

All hybrid scenarios show better results in terms of $LL_\%$ and $OP_\%$ with respect to the corresponding single-component scenarios, confirming the usefulness of a complementary hybrid ESS. A relevant reduction in $LL_\%$ can be achieved for hybridised scenarios: in particular a reduction equal to 16% is achieved for the hybridised battery-priority scenario compared to the battery-only scenario, and a reduction equal to 9% is achieved for the hybridised H$_2$-priority scenario with respect to the H$_2$-only scenario. A less relevant reduction of $OP_\%$ is achieved, with a 3% and 1% reduction of the $OP_\%$ for battery and hydrogen hybridised scenarios respectively, with respect to their respective single-component scenarios.
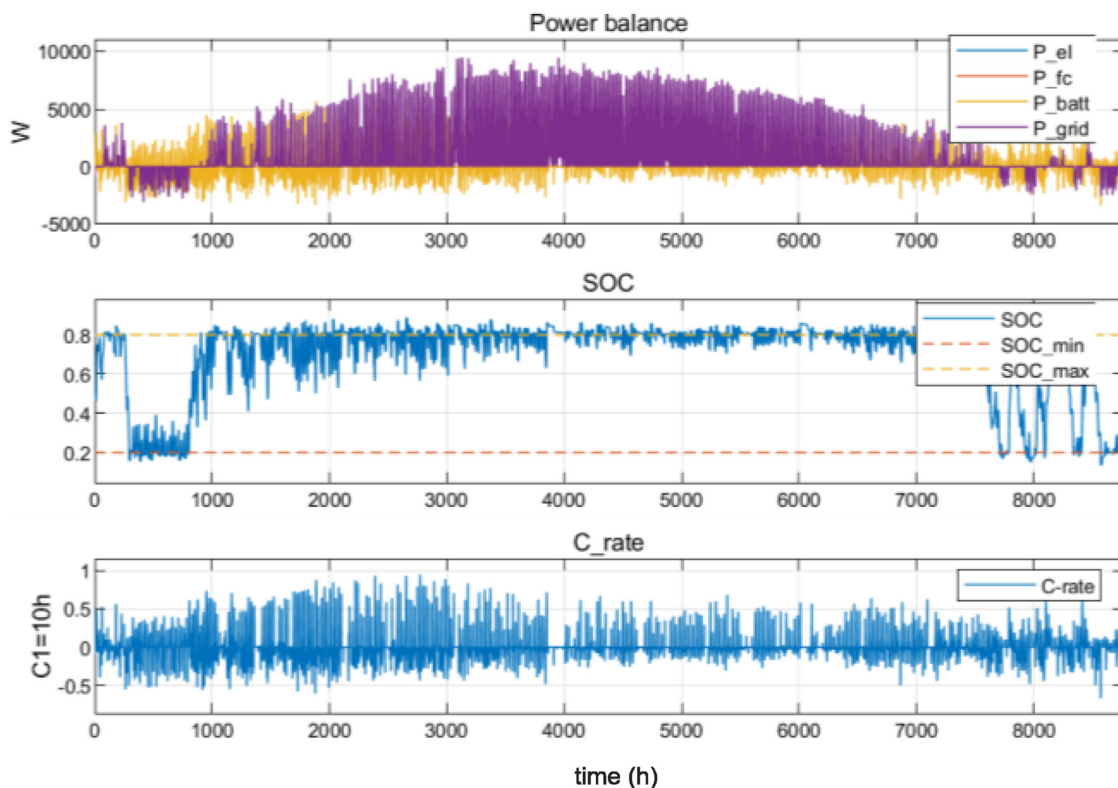
Fig. 10. Yearly (battery-only) simulation. (Top) power balance (W); (medium) battery SOC (%); (bottom) battery C-rate. Parameters: Q_{batt}=100 Ah; V_{tank}=0 m^3=0 Nm^3.
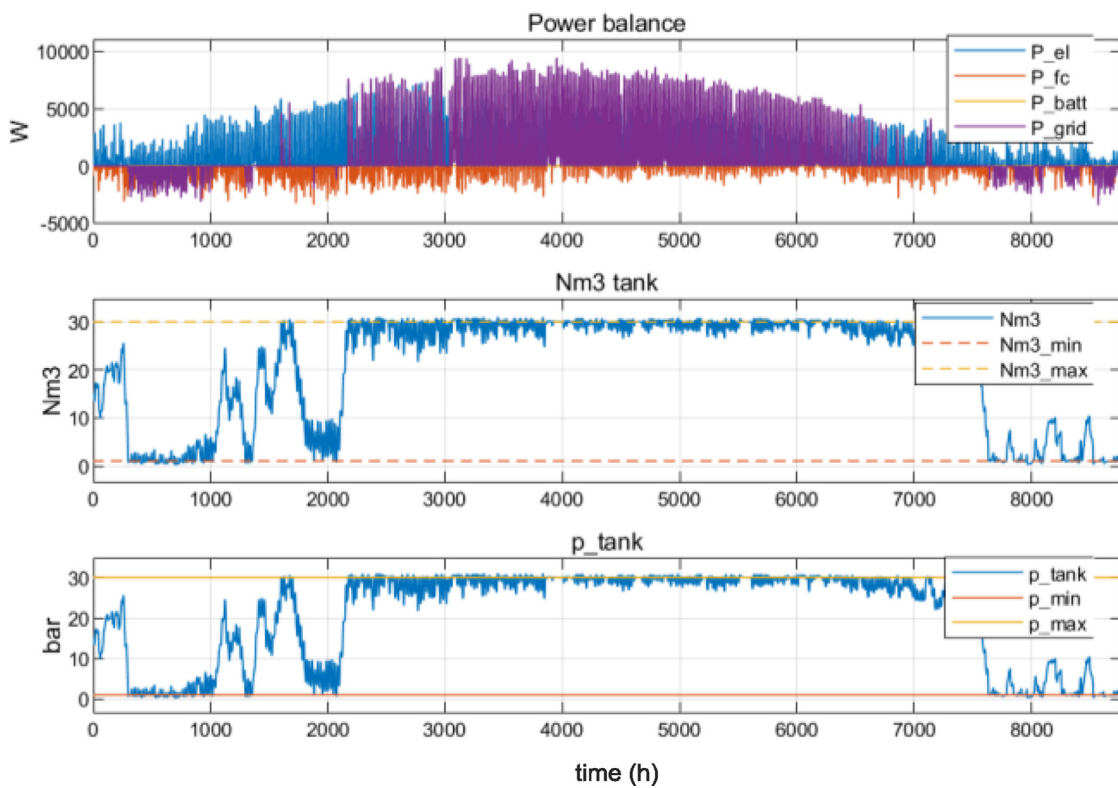

Fig. 11. Yearly (H$_2$-only) simulation. (Top) power balance (W); (medium) H$_2$ vol V_{tank} (Nm^3); (bottom) H$_2$ tank pressure p_{tank} (bar). Param.: Q_{batt}=0 Ah; V_{tank}=1 m^3=30 Nm^3.
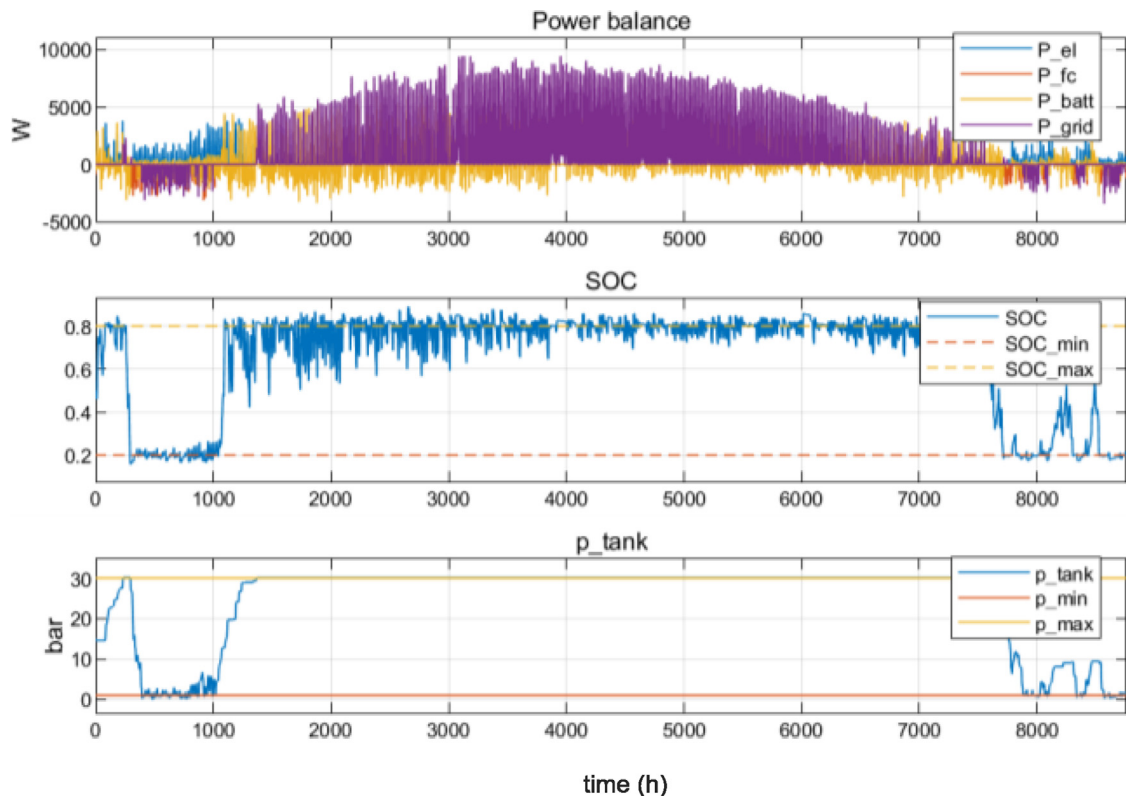
Fig. 12. Yearly (hybrid battery-hydrogen) simulation with battery-priority EMS. (Top) power balance (W); (medium) battery SOC (%); (bottom) H_2 tank pressure p_{tank} (bar). Parameters: Q_{batt}=100 Ah; V_{tank}=1 m^3=30 Nm^3.
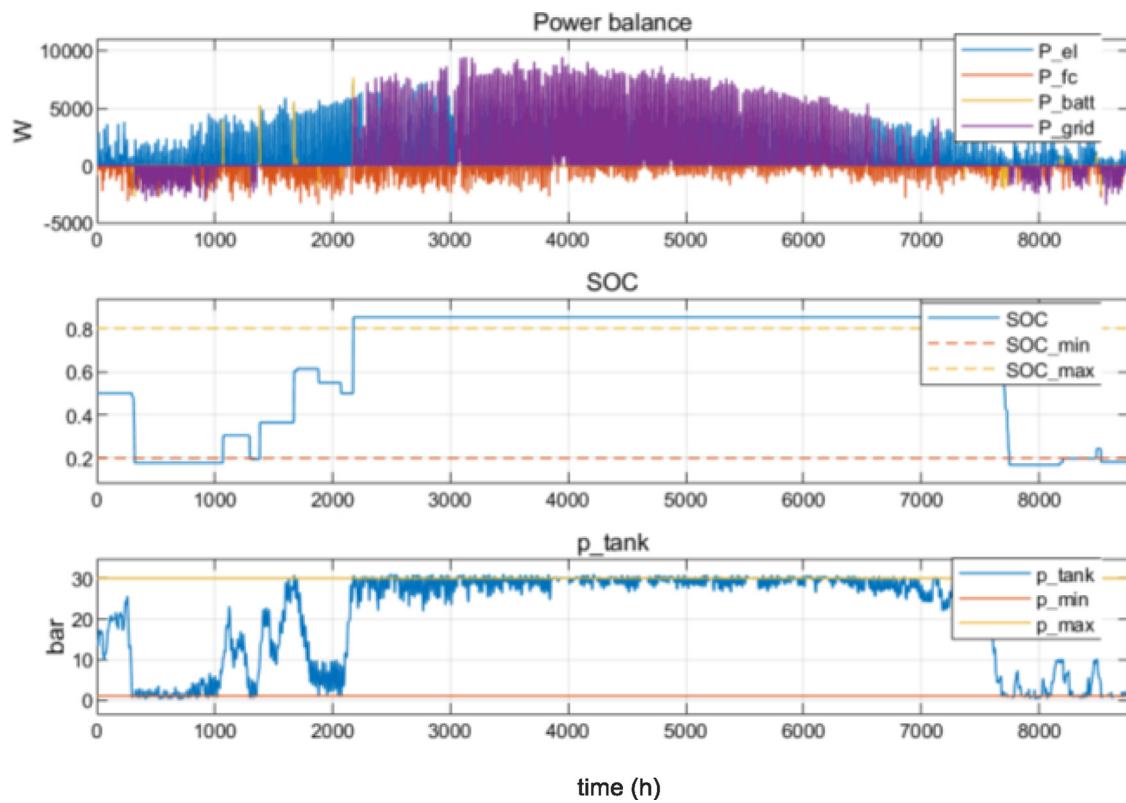

Fig. 13. Yearly (hybrid battery-hydrogen) simulation with H_2-priority EMS. (Top) power balance (W); (medium) battery SOC (%); (bottom) H_2 tank pressure p_{tank} (bar). Parameters: Q_{batt}=100 Ah; V_{tank}=1 m^3=30 Nm^3.
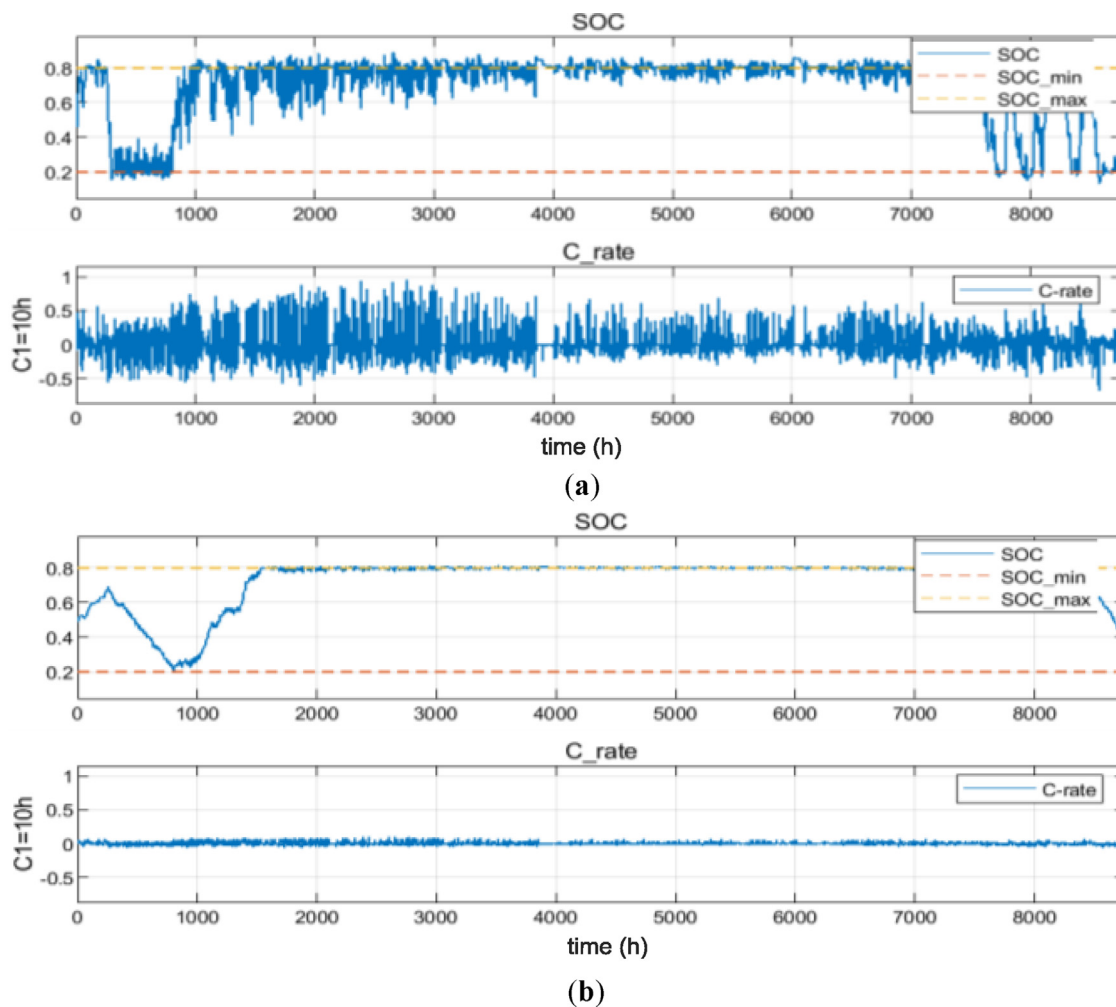
A. Monforti Ferrario, A. Bartolini, F. Segura Manzano et al.

Advances in Applied Energy 3 (2021) 100048

Fig. 14. Yearly (battery-only) simulation. Battery SOC (%) & battery C-rate. (a) Q_{batt}=100 Ah; (b) Q_{batt}=1000 Ah.

4.1.1. Single-component ESS parametric analysis results – battery-only and H_2-only

The variation of scale of the ESSs determines a series of superposed effects on the response of the microgrid storage: for example a battery bank with a larger capacity induces operation at lower C-rate, thus presenting a reduced amplitude variation of the SOC which shows a more continuous trend; an increased energy (thus increased time at equal P_{net}) is required to increase/decrease the SOC of an equal amount. Instead, a battery bank with a smaller capacity will operate under higher C-rate, which induces a greater SOC amplitude variation and a smaller amount of energy (thus less time at equal P_{net}) determines a significant variation of the SOC which presents a more discrete step-like trend [78]. Fig. 14 illustrates such effect comparing the SOC and C-rate of two battery-only simulations (Q_{batt}=100 Ah and Q_{batt}=1000 Ah, respectively).

A similar effect is obtained by the increasing/decreasing of V_{tank} (Fig. 15), which modifies the hydrogen tank capacity (therefore the H_2 mass which can be stored at equal nominal pressure) and the system autonomy. In addition, the maximum load threshold is modified with scale.

For the single-component ESS simulation scenarios Fig. 16 reports the trends of the output parameters LL and OP (and their percentages) with the increase of scale. The increase of battery capacity results in a stronger reduction of the LL from around 2 MWh/year ($LL_\%$ equal to 20%) at low capacity (<50 Ah) up to near-zero values at 700 Ah (i.e. 250 kWh stored). However the LL improvement easily reaches a plateau for large capacities for which further increase of battery capacity does not provide positive effects in terms of energy supplied [79]. Instead,

the increase in H_2 storage capacity leads to a less steep reduction of the LL with an almost linear tendency at medium capacity ranges between 1 and 8 m^3 (i.e. 50–275 kWh stored) after a sharp decrease at lower volumes (<1 m^3). The minimum LL is around 0.17 MWh/year ($LL_\%$ equal to 3%), around 15% of the initial value at low tank capacity (V_{tank} equal to 0.5 m^3).

Similar challenges in autonomous H_2 operation are found in literature [80], where even with a relevant increase of the hydrogen storage capacity this must be supported by an external support unit (e.g. genset).

The different behaviour of the H_2 system can be explained by a multitude of overlapping factors. Firstly, the H_2 ESS (at equal capacity) presents lower round-trip efficiency compared to the battery ESS (see Table 8). Secondly, the PEMFC at nominal operating conditions consumes approximately 3 times the hydrogen produced by the electrolyser in the same time period, leading to an inconsistent management of the tank and the limited maximum storage volume and allowed pressure range of the tank (operated between 10 and 20 bar) does not allow sufficient flexibility without quickly reaching saturation. On the other hand, the battery bank can be operated at highly variable C-rates (up to 5C) and the net power can be always stored or withdrawn also at low battery capacities, provided that the SOC is maintained within the suitable operating range limits. Also, the SOC allowed operating range is slightly wider (20–80% of the maximum capacity) than the p_{tank} operating range (10–20 bar which equates to 33–66% of the maximum pressure), providing increased flexibility capability to the battery system at equal stored energy capacity.
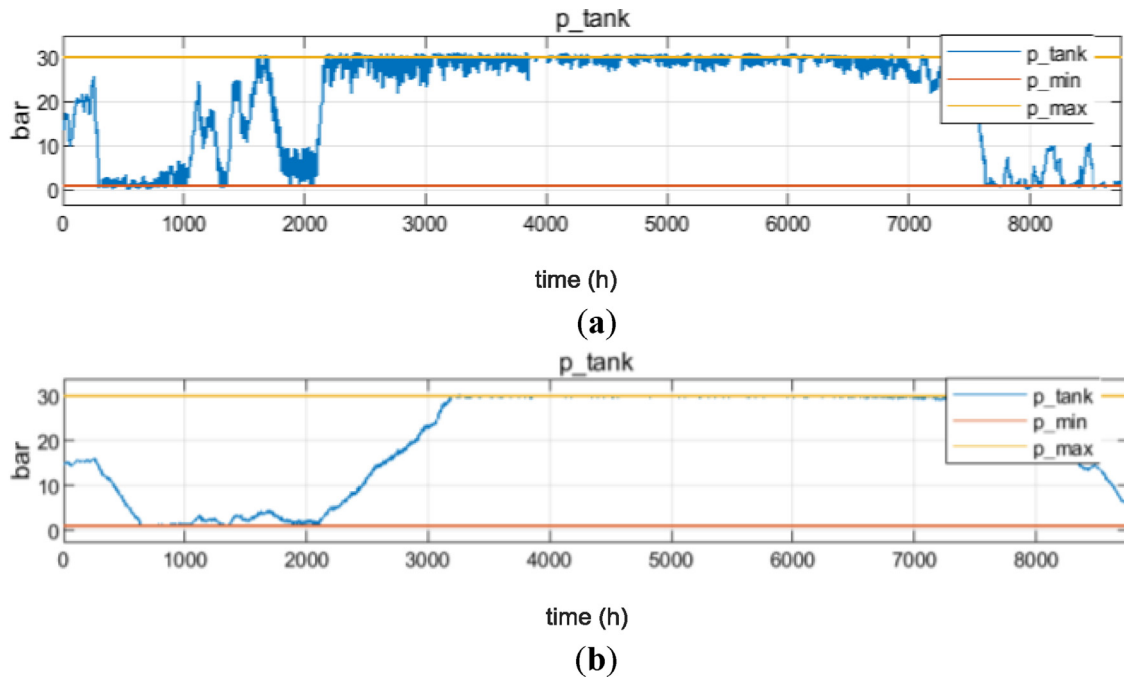
A. Monforti Ferrario, A. Bartolini, F. Segura Manzano et al.

Advances in Applied Energy 3 (2021) 100048

Fig. 15. Yearly (H_2-only) simulation. H_2 tank pressure p_{tank} (bar). (a) V_{tank}=1 m^3=30 Nm^3 (top); (b) V_{tank}=10 m^3=300 Nm^3 (bottom).
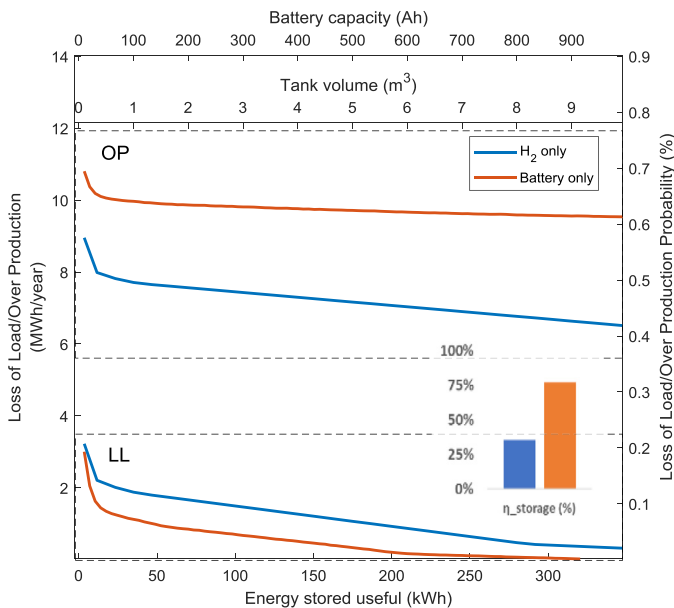

Fig. 16. Performance parameters versus storage capacity (single-component).

For OP, the opposite happens: the H_2-only scenario shows lower OP values overall respect to the battery-only scenario and an increase in H_2 capacity induces a more relevant OP decrease (27% reduction from 9.53 MWh/year to 6.97 MWh/year) of the OP compared to an increase in battery capacity (12% reduction from 11.28 MWh/year to 9.96 MWh/year). Both trends show a sharp drop in OP at low capacity (<25 kWh stored) then follow a linear trend. The slope of the H_2-only configuration is steeper than the battery-only one due to the capacity of the H_2 ESS to absorb larger amount of energy continuously without saturating the storage tank. However, due to the lower round-trip efficiency, this is counterbalanced by increased losses.

The round-trip storage efficiency strongly depends on the ESS technology, resulting in average equal to 36% for the H_2 ESS and 76% for the battery ESS.

4.1.2. Hybrid ESS parametric analysis results – battery-priority EMS

The simulation results of hybrid battery-H_2 scenario – battery-priority EMS – show that the LL and $LL_\%$ (Fig. 17- top), as previously shown in Fig. 16, are slightly more affected by the increase of battery capacity (around 10% reduction on each incremental step) rather than by the hydrogen tank volume (around 5% reduction on each incremental step), however their variability range is limited in absolute value since the overall LL is limited to below 550 kWh/year (worst case with Q_{batt}<200 Ah and V_{tank}<1m^3). With moderate ESS scales (Q_{batt}>300 Ah and V_{tank}>3 m^3) the $LL_\%$ can be limited to well below 5%, reaching zero value for the whole upper half of the analysed ESS variability envelope.

The OP and $OP_\%$ (Fig. 17- bottom) show higher overall values (OP between 8.8–10.2 MWh/year; $OP_\%$ between 54 and 63%) and a more marked dependency on the H_2 tank volume increase (up to 9–12% reduction) with respect to the battery capacity (up to 1–5% reduction) due to the greater energy volume processed by the H_2 ESS, albeit with greater losses. $OP_\%$ is reduced from 63% for low ESS capacity to a minimum of 54% for the maximum tank capacity (10 m^3) and half of the maximum battery capacity (500 Ah).

The non linear variation of OP with increasing battery capacity can be justified as follows. For battery capacities which are too low (<500 Ah) the energy capacity is too small leading to a greater variation of the SOC which quickly surpasses the control limits, resulting with an often unavailable battery. For battery capacities which are too high (>500 Ah) the battery system may persist within the hysteresis bandwidth amplitude: after becoming unavailable the SOC cannot reach the restoration limit imposed by the hysteresis band, reason for which the EMS logic considers it unavailable. This phenomenon can be clearly seen in the simulation reported in Fig. 18 (Q_{batt}=750 Ah; V_{tank}=10 m^3=300 Nm^3), where the battery SOC remains between 20 and 30% between 2100 and 2500 h, preventing the battery to absorb the net power. This example highlights the importance of the hysteresis bandwidth amplitude in microgrid operation [68]. Also other literature studies report the non-linear behaviour of performance parameters as a function of battery capacity, which alters the balance between perfectly met load (which needs a large battery capacity) and inconsistent use of either the solar resource or the fuel cell component [30,38,42].
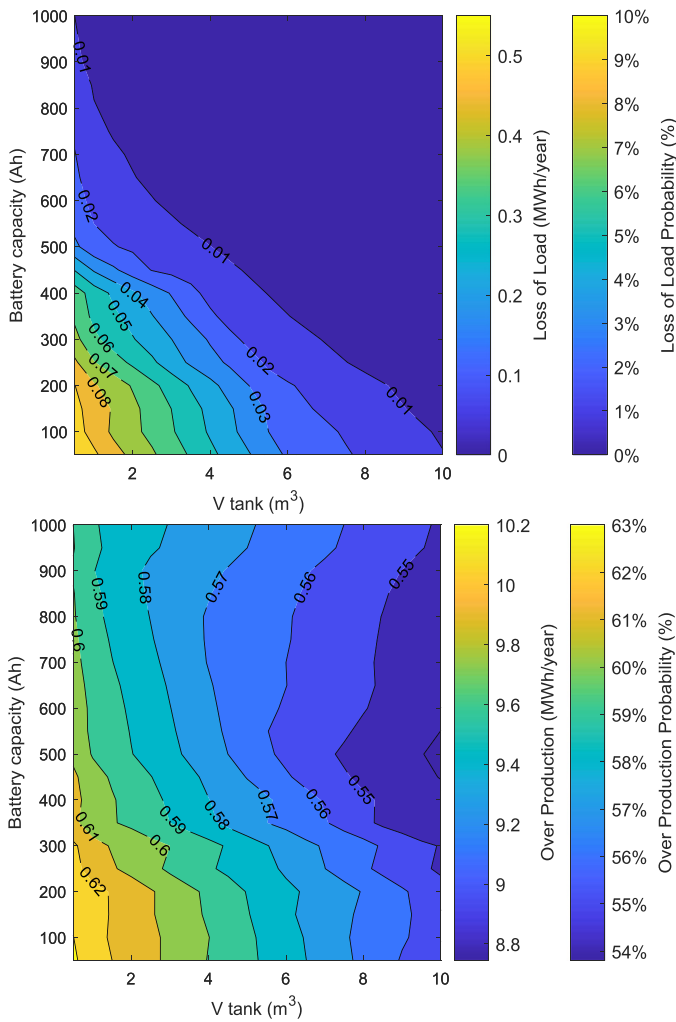
Fig. 17. LL and LL$_\%$ (top); OP and OP% (bottom) vs storage capacity (hybrid battery-hydrogen – battery-priority EMS).

A further reduction of OP below 9 MWh/year (OP$_\%$ equal to 54%) is hard to obtain with the battery-priority EMS due to the strong summer overproduction unbalance shown in Fig. 8, which is challenging to absorb even by increasing both ESS to their maximum capacity. Both systems easily reach oversaturation and deep discharge does not occur until the end of summer (September-October).

Also the storage efficiency η_{ESS} (Fig. 19) follows a non-linear behaviour caused by the perduring hysteresis state of the battery bank. Overall the η_{ESS} range is within 50–70%, with a strong decreasing trend with the reduction of the hydrogen tank capacity, due to the increased utilization of the battery system, which presents higher round-trip efficiency values (average battery single component round-trip efficiency equal to 76%).

4.1.3. Hybrid ESS parametric analysis results – H$_2$-priority EMS

For the hybrid battery-H$_2$ scenario – H$_2$-priority EMS – the LL and LL$_\%$ results (Fig. 20- top) show a linear trend with respect to the increase of the hydrogen tank, whereas a slight non-linear behaviour can be observed with the variation of the battery capacity. The LL ranges from around 700 kWh/year (LL$_\%$ equal to 12%) for very low values of ESS capacity (V$_{tank}$<1 m^3 and Q$_{batt}$<100 Ah) up to near-zero values for combinations with higher ESS capacity (V$_{tank}$<7.5 m^3 and Q$_{batt}$<400 Ah).

Overall, the LL and LL$_\%$ values under H$_2$-priority EMS are higher than those obtained under the battery-priority EMS (maximum LL and

Table 9
Single-component cost optimization results.

LL$_\%$	Total cost (k€)	Q$_{batt}$ (Ah)	E$_{ESS,useful}$ (kWh)	OP$_\%$ (%)	η_{ESS} (%)
Battery-only					
10%	90.7	40	13.6	64.9%	75.62%
5%	108.6	290	98.6	63.1%	75.79%
1%	193.8	790	268.6	61.7%	74.97%
H$_2$-only					
10%	163.5	3.33	115.2	48.6%	36.36%
5%	174.3	7.33	253.5	45.2%	36.67%
1%*	–	–	–	–	–
* H$_2$-only configuration does not reach LL$_\%$ equal to 1% within the search space					

LL$_\%$ equal to 550 kWh/year and 9% respectively). In fact, the increased utilization of the hydrogen systems imposed by the EMS entails a greater LL (especially during critical load demand during winter) since the H$_2$ systems present lower round-trip conversion efficiency and the energy stored by the electrolyser is insufficient for the fuel cell to supply the demand. Also inconsistent tank management in terms of maximum storage volume and limited operating pressure range affects negatively the H$_2$ ESS with regard to the LL. Unlike the battery-priority EMS, a reduced portion of the search space achieves near-zero values and zero LL values are never reached, even with high ESS capacity conditions.

The OP results (Fig. 20- bottom) range between 6.5 and 8.5 MWh/year (OP$_\%$ equal to 40–55%) for different ESS combinations. The trend presents a rather linear reduction with the increase of V$_{tank}$, with an average decrease of OP of around 17% across the whole analysed range (0.5–10 m^3); the increase of the battery capacity Q$_{batt}$ induces a less steep reduction of OP up to around 5% across the analysed range (50–1000 Ah).

The H$_2$-priority EMS presents lower OP and OP$_\%$ values (between 6.5–8.5 MWh/year) respect to the battery-priority EMS (between 8.8–10.2 MWh/year). H$_2$-priority EMS also presents higher OP reduction rates (17% reduction with increasing V$_{tank}$ and around 5% reduction with increasing Q$_{batt}$) compared to the battery-priority EMS (9–12% reduction with increasing V$_{tank}$ and between 1 and 5% reduction with increasing Q$_{batt}$). In particular the reduction rate with respect to the V$_{tank}$ is more pronounced due both to the increased amount of energy processed by the H$_2$ ESS – counterbalanced by increased losses – and the less frequent use of the battery systems.

The analysis of the storage efficiency (Fig. 21) shows a rather constant η_{ESS} around 40% across the whole capacity range, with a slight increasing trend in larger battery capacity scenarios with small hydrogen capacities (top-left corner). Respect to the battery-priority case, the increase in η_{ESS} with increasing battery capacity is limited, since the EMS will prioritize the use of the H$_2$ ESS instead. Overall, the average is much lower respect to the battery-priority case, since the average round trip efficiency of the hydrogen systems is lower, equal to 36%.

4.2. Cost optimization results for target LL$_\%$ thresholds

The total storage cost optimization results for single-component and hybrid configuration is analysed for LL$_\%$ threshold values equal to 10%, 5% and 1% (although lower LL$_\%$ values can be reached). The reported total storage cost is calculated via Eqs. (12) to 15.

While for single-component scenarios a unique storage configuration is found and reported in Table 9, for hybrid ESS scenarios a plethora of different Q$_{batt}$/V$_{tank}$ configurations can complementarily obtain the same overall LL$_\%$ – as shown in Fig. 22. With the parametric analysis approach the total storage cost of each configuration which lies within the ±0.5% range of the desired LL$_\%$ threshold must be calculated and compared to individuate the cost optimal configuration. This approach is fully deterministic and less efficient in terms of computational load: considering that a single yearly simulation lasts around 5–10 s, the optimal search can computation time is in the range of 10,000–20,000 s (several hours) for each EMS configuration with 2000 possible config-
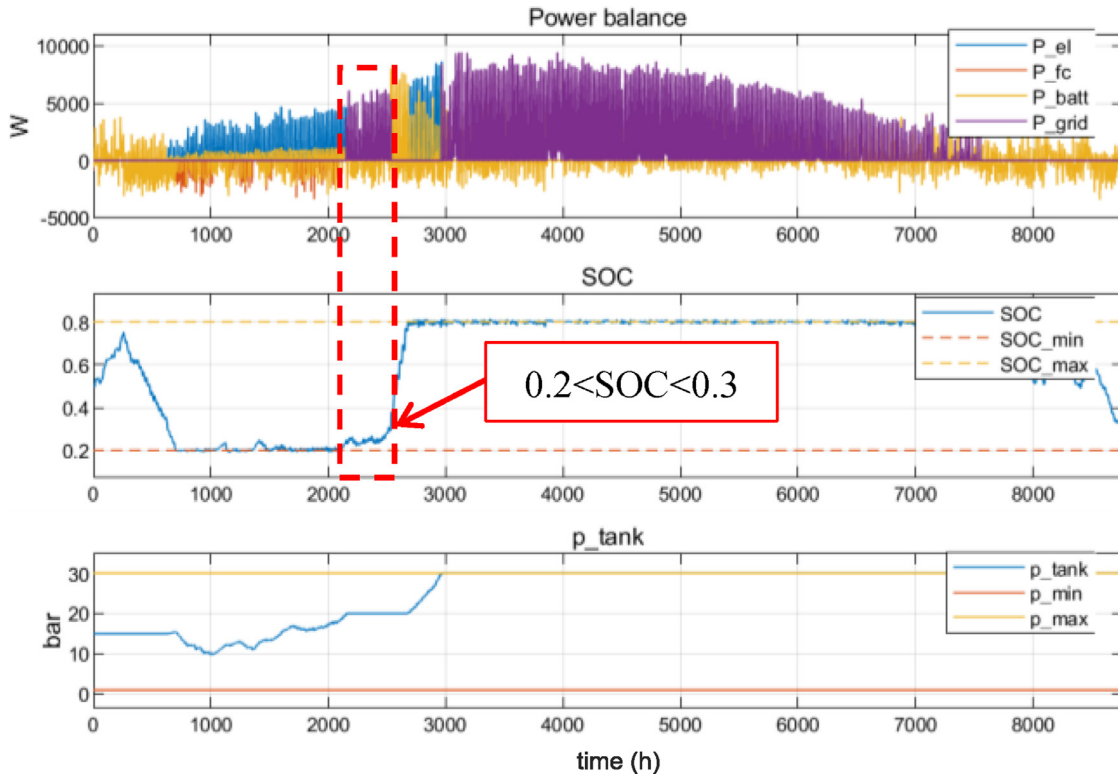
A. Monforti Ferrario, A. Bartolini, F. Segura Manzano et al.

Advances in Applied Energy 3 (2021) 100048

Fig. 18. Yearly simulation with battery-priority EMS. Parameters: Q_{batt}=750 Ah; V_{tank}=10 m^3=300 Nm^3; $P_{el,nom}$=10 kW$_e$; $P_{fc,nom}$=10 kW$_e$.
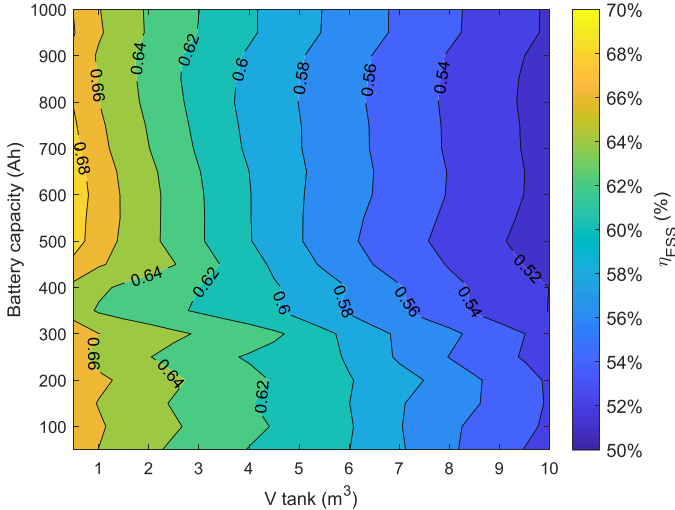

Fig. 19. Storage efficiency η_{ESS} versus storage capacity (hybrid battery-hydrogen – battery-priority EMS).

urations for each LL$_\%$ threshold. The same result can be obtained via the PSO algorithm which converges to the minimal cost configuration for the chosen LL$_\%$ constraint. Obviously the computation time with the PSO algorithm is reduced to the range of 1000s (few minutes) since convergence to the optimal solution is reached after approximately 25 iterations for the two EMS scenarios (around 625 simulations, considering the swarm size given in Table 7), but the result does not provide information on the sub-optimal regions.

Generally, the storage cost increases with the decrease of the LL$_\%$ due to increasing stored energy requirements. The battery-only scenario requires relevantly less useful stored energy compared to the hydrogen-only scenario, due to differences in nominal round-trip effi-

ciency and operational behaviour previously explained. In fact 13.6 kWh and 98.6 kWh of energy stored in the battery system are required with respect to 115.2 kWh and 253 kWh for LL$_\%$ equal to 10% and 5% respectively. As expected, the battery-only scenario storage cost is lower (91/108 k€ for 10%/5% LL$_\%$ respectively), due to the lower size of the battery system and lower LL penalization; instead, the H$_2$-only scenario total storage cost (163/174 k€ for 10%/5% LL$_\%$ respectively) is penalised by a fixed cost of electrolyser and fuel cell also for small tank sizes. The comparison at LL$_\%$ equal to 1% cannot be performed since the H$_2$-only system does not reach such value in the analysed search space.

The storage efficiency of the optimal sizing configurations for each LL$_\%$ thresholds are very similar to the average η_{ESS} values in single component scenarios (Fig. 16) since the variation range for η_{ESS} with size is quite limited.

Although penalisation cost is high (VoLL equal to 8.7 €/kWh) the analysis of operation towards island mode means that LL energy volumes are low (in most cases <1 MWh/year, see Fig. 15, 16 & 19), leading to a maximum energy cost of under 10 k€/year for most configurations. This means that the total storage cost is mainly composed of CAPEX & OPEX of the ESS components rather than the penalization cost for the lost commodity.

Analysing the identified combinations of ESS configurations reported in Fig. 22 it is clear that battery-priority EMS requires lower stored energy and therefore lower cost, due to the increased use of batteries which – for previously discussed reasons – is more suitable to limit the LL$_\%$ and higher η_{ESS}. Amongst the identified combinations the cost optimization search tends to always prefer an increase in V_{tank} rather than one in Q_{batt} since – considering the selected economic parameters reported in Table 6 – the hydrogen system presents a lower marginal cost per additional unit of stored useful energy (2000 €/kg which equates to 161.6 €/kWh$_{useful}$ considering the LHV of hydrogen and the round trip efficiency of 37.5%) compared to the battery system (235 €/kWh$_{useful}$ considering the round trip efficiency of 85%); in fact, the electrolyser and fuel cell (both fixed at 10 kW$_{e,nom}$ for all configurations) represent
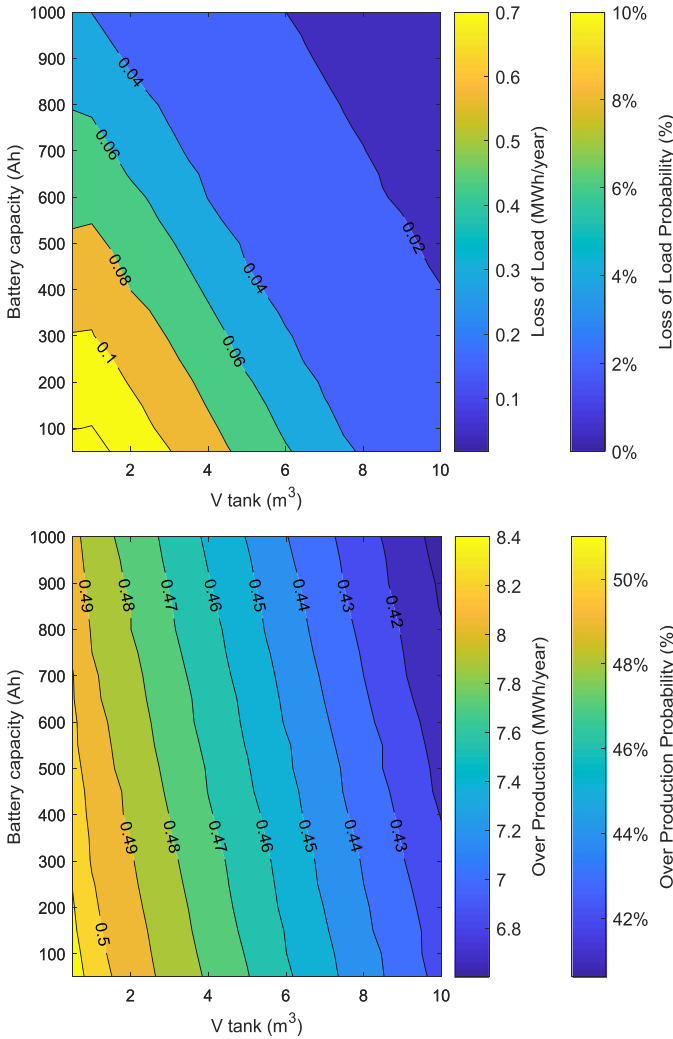
A. Monforti Ferrario, A. Bartolini, F. Segura Manzano et al.

Advances in Applied Energy 3 (2021) 100048

Fig. 20. LL and LL$_\%$ (top); OP and OP% (bottom) versus storage capacity (hybrid battery-hydrogen – H$_2$-priority EMS).
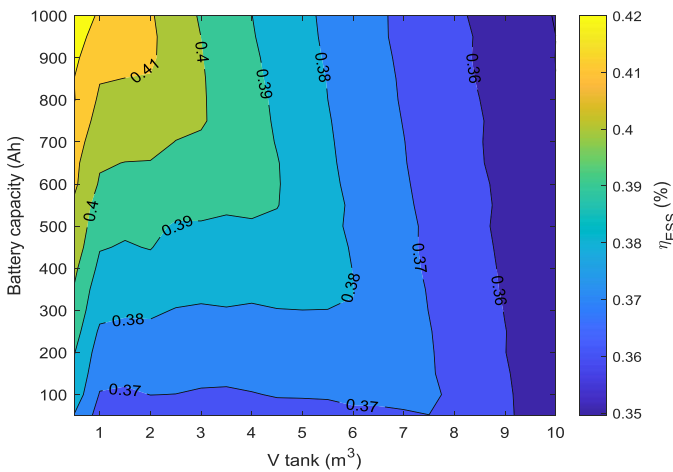

Fig. 21. Storage efficiency η_{ESS} versus storage capacity (hybrid battery-hydrogen – H$_2$-priority EMS).

a fixed cost for both EMS and do not shift the economic balance from one EMS to the other.

The cost optimal configurations of hybrid scenarios reported in Fig. 23 (found by either parametric analysis or PSO algorithm) show a similar trend for to single-component scenarios (Table 8): total storage cost increases with decreasing LL$_\%$ and H$_2$-priority EMS cost optimal configurations show a poorer performance in terms of η_{ESS} (around 35–37% vs. 54–70%), useful stored energy (121/259/549 kWh$_{useful}$ vs. 35/155/328 kWh$_{useful}$) and total storage cost (140/185/326 k€ vs. 110/150/208 k€) compared to the battery-priority EMS for all cases. The η_{ESS} decreases with decreasing LL$_\%$ since the ESS are used more intensively.

It should be pointed out that although hybridisation has been shown to be always useful from an energy perspective (see Section 4.1), the cost optimal solutions for hybrid ESS scenarios are not always improved vis-à-vis to the respective single-component scenario, confirming that energy and economic objectives do not coincide.

The economic results are aligned with the reviewed literature in which hybrid energy systems are analysed as a function of the reduction of LL$_\%$. In general, the commonality to all reported works is that system performance and cost is stressed when low LL$_\%$ are searched. A qualitative comparison of the present work with other comparable specific contribution is given in Table 10, in terms of analysed LL$_\%$ range and effect in varying the LL$_\%$.

The consideration of variable P$_{el,nom}$ and P$_{fc,nom}$ and/or their adaptation to the tank size could significantly shift the economic balance of the hybrid configuration and provide an updated cost trade-off [30,38]. Also, the maximum potential cost saving (which is equal to 30 k€ considering the specific investment costs indicated in Table 6) would affect both hybrid system configurations in which the systems are present, without relevantly affecting the general conclusions that can be drawn from the cost trends in Fig. 23 which differ due to the EMS rather than the CAPEX of the systems.

Also the inclusion of a revenue stream from electricity sale could affect the H$_2$-only scenario, since it presents significantly lower values of OP% (around 45–48%) respect to the battery-only scenario (around 60–65%). Both aspects are deemed relevant by the authors and will be object of future work.

5. Concluding remarks

In this paper a model-based analysis of the optimal design of a hybrid battery/hydrogen storage of a RES microgrid connected to a residential load in simulated off-grid conditions is carried out. The simulative tool implemented for this analysis is a detailed, component-oriented model, which was previously developed and validated with experimental data by the authors. At system level, four Energy Storage Systems ESS configuration scenarios (battery, H$_2$, hybrid battery-H$_2$ with battery priority, hybrid battery-H$_2$ with H$_2$ priority) have been simulated and analysed under different EMS. The results are analysed via performance parameters such as Loss of Load LL, Over Production OP, round-trip storage efficiency η_{ESS} and total storage cost C$_{tot,ESS}$. A parallel approach to the optimal design of the storage capacity is carried out via multi-dimensional parametric analysis and Particle Swarm Optimization PSO, which can both identify the optimal combination of the two design variables related to the storage energy capacity (Q$_{batt}$ and V$_{tank}$, in the range of 0–350 kWh$_{useful}$) with decreasing LL$_\%$ thresholds (from 10% to 1%), toward fully islanded conditions (LL$_\%$ equal to 0%). The parametric analysis provides useful information regarding the trends of the performance parameters with the design variables, (which is key to understand the dynamics of the energy management in RES microgrids), other than only the optimal point, provided by the PSO approach.

From the results, some general and specific conclusions can be drawn. The general conclusions are consequence of the operational characteristics of the two storge technologies (battery or H$_2$ storage, respectively) thus can be extended to other comparable plants as well.
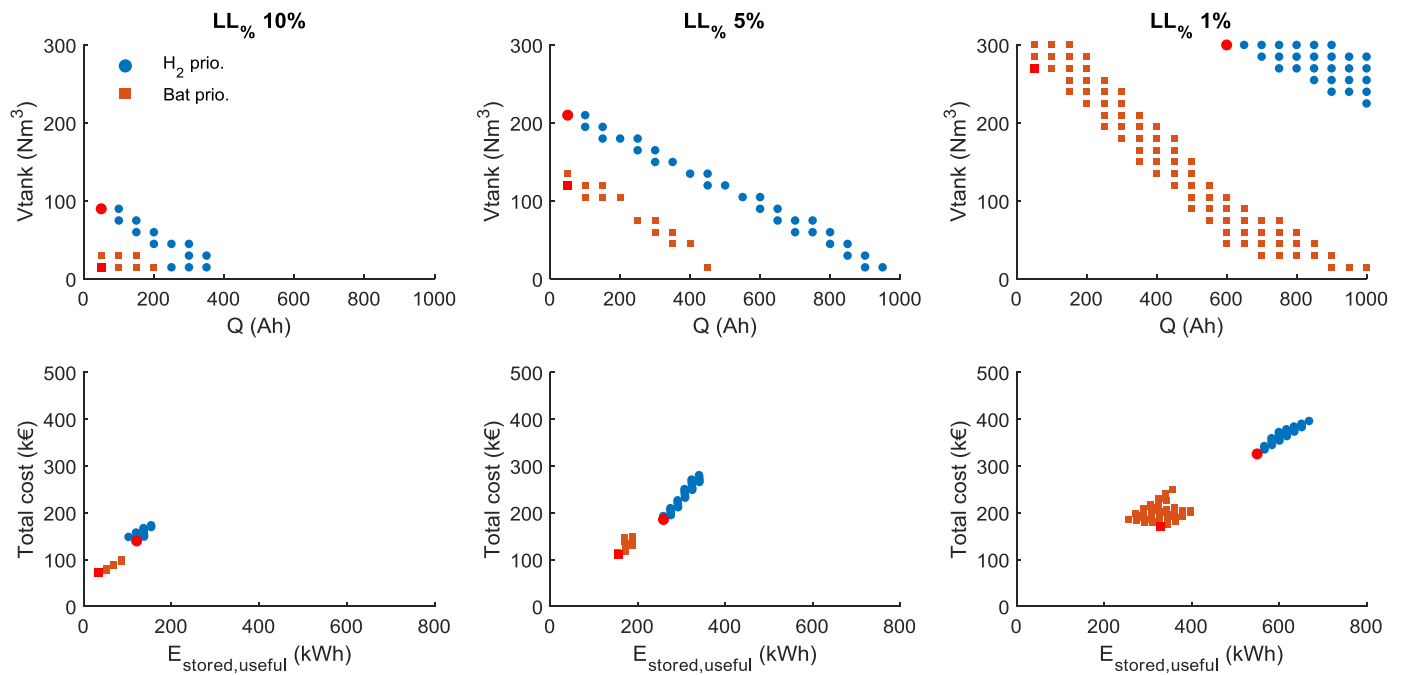
Fig. 22. Identified ESS configurations (**top**) in terms of battery capacity (Ah) and tank volume (Nm³) and (**bottom**) total cost (k€) versus useful energy stored (kWh) of possible hybrid ESS by $LL_\%$ (10%/5%/1%) threshold and EMS (**red markers** indicate the identified cost-optimal configuration obtained by PSO technique).

Table 10
Comparison of the results of the present work with reviewed literature.

|	$LL_\%$ range	Analysed effect of $LL_\%$
Authors' proposal	0–10%	Impact on energy supply, stored energy & Cost of Storage and for sizing optimization
Eltamaly et al. [26]	0–100%	Impact on Cost of Energy with load prioritization
Semaoui et al. [17]	1–3%	Impact on State Of Health of battery and lifetime
Serra et al. [38]	0–5%	Impact of Self Sufficiency Ratio on Cost of Energy
Rozzi et al. [77]	0–5%	Pareto front for NPC for sizing optimization
Hafez et al. [37]	0–10%	Impact on energy supply for sizing optimization
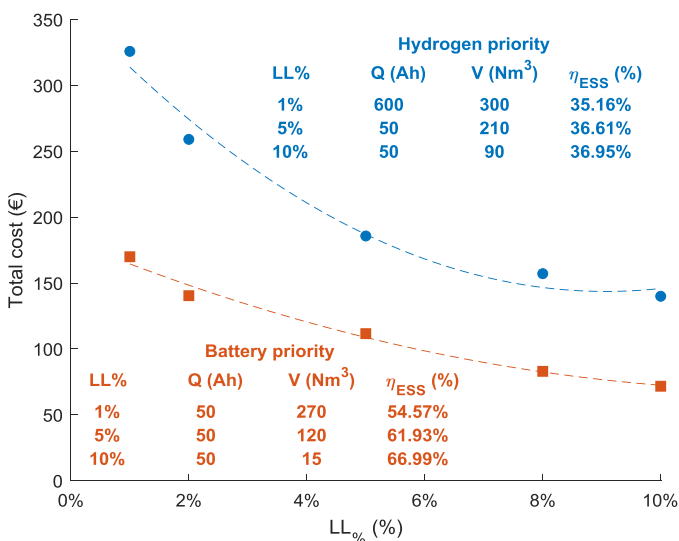
Fig. 23. Cost-optimal configurations of hybrid ESS scenarios by $LL_\%$ threshold and EMS: H_2-priority (solid blue line); battery-priority (solid orange line).

Even in highly oversized PV environments for both power and energy, 100% RES supply to domestic users is challenging. Achieving zero LL throughout the year (pure stand-alone mode) entails the installation of large-sized ESS (Q_{batt}>500–600 Ah for battery only and battery-priority scenarios, hardly reached in hydrogen scenarios, even for high values of V_{tank}) which are costly and complex to manage. In addition, given the PV driven RES generation which is hard to couple with the residential load profile, the achievement of low values of LL (around 1–10%) usually entails high values of OP (around 50–60%) which represent large volumes of renewable energy not used locally, wasting the added value that locally distributed RES generation could potentially provide.

While sizing storage systems the actual requirements of energy security of the demand should be taken into account. In fact, an allowable $LL_\%$ threshold induces a substantial relaxation of the storage systems' capacity and cost requirements (e.g. 50–55% reduction in energy capacity and 30–45% reduction in total storage cost by increasing the $LL_\%$ threshold from 1% to 5%). A trade-off should be found with respect to acceptable $LL_\%$ levels and total storage cost.

In general an increase of ESS size induces a positive effect in the energy security performance parameters, especially at smaller scale for which the $LL_\%$ and $OP_\%$ reductions are steeper, despite a loss in energy efficiency due to the round-trip storage efficiency and an increase in cost.

Hybridisation of hydrogen with batteries is always advantageous from an energy security perspective compared to single-component ESS scenarios (as shown in Table 8), allowing to exploit the different systems in a complementary way. However, storage efficiency and cost are negatively affected by hydrogen storage in hybrid scenarios, demonstrating that energy security, storage efficiency and cost objectives do not coincide.

A. Monforti Ferrario, A. Bartolini, F. Segura Manzano et al.

Advances in Applied Energy 3 (2021) 100048

A battery-based ESS seems more suitable for short term storage with daily charge/discharge dynamics. In fact, the battery-based scenarios present lower $LL_\%$ (zero LL with Q_{batt} around 500–600 Ah) with higher round-trip storage efficiencies (around 60–70%), although presenting higher $OP_\%$ values (above 50–60%). From an economic point of view the incremental cost in terms of additional energy capacity (€/kWh$_{useful}$) is high, since the whole battery bank must be upsized and the optimal search tends to prefer lowest size battery capacity which can guarantee the given $LL_\%$ threshold.

On the other hand, hydrogen storage seems likely to be more suitable for long-term storage scenarios, being able to process and store higher energy volumes. The results of H_2-based scenarios show a reduction in $OP_\%$ (around 40%, lower by 20% respect to the battery scenarios) but worse results in terms of $LL_\%$ (up to 5% more) and storage efficiency (around 35–37% due to the lower η_{ESS} of the hydrogen systems). From a cost point of view the hydrogen conversion systems (electrolyser and fuel cell) represent a high CAPEX contribution, but the storage tank shows a low incremental cost in terms of additional energy capacity (€/kWh$_{useful}$). For this reason the search algorithm tends to chose a larger storage tank capacity which provides that specific $LL_\%$ threshold, minimizing the increase in battery capacity.

The cost-optimal configurations show a total storage cost (20 years operation) between 90 and 200 k€ for the battery-based scenarios and between 150 and 300 k€ for the H_2-based scenarios, showing that currently H_2 storage is still relevantly more expensive with respect to battery storage, although the downsizing of the electrolyser and fuel cell nominal power could reduce the gap. Also in terms of useful stored energy the cost-optimal configurations of hydrogen-based scenarios require more storage capacity respect to battery-based scenarios (121/259/549 kWh$_{useful}$ vs. 35/155/328 kWh$_{useful}$ for 10%/5%/1% $LL_\%$ respectively). The economic competitiveness of H_2 storage could be enhanced with longer-term storage horizons (monthly, seasonal, etc.), where the lower marginal cost of the storage tank could be advantageous.

All in all, this paper provides an innovative contribution to optimal storage design of an actual hybrid battery/hydrogen storage coupled to a RES microgrid which supplies a real residential load profile. The demonstrated parallel optimization approach represents a successful testing of the validity of the results obtained by the numerical PSO algorithm without neglecting the energy aspect with the rigorous systematic approach of the parametric analysis. For a more comprehensive optimization analysis of the whole microgrid environment, the variation of more parameters (such as the installed power of electrolyser and fuel cell, other than battery characteristics and RES generators) should be implemented together with the analysis of additional performance indicators with a multi-objective optimization approach, which will be object of future work. Other active energy management approaches such as load priority repartition, demand side flexibility or load shedding/shifting could potentially be advantageous in the analysed conditions.

6. Acronyms

A/C: Air Conditioning
CAPEX: Capital expenditures
DHW: Domestic Hot Water
EMS: Energy Management Strategy
ESS: Energy Storage Systems
GHI: Global Horizontal Irradiance
HH: Hub Height
LHV: Lower Heat Value
LL: Loss of Load
MEB: Minimum Energy Building
OP: Over Production
OPEX: Operating expenses
PEMFC: Proton Echange Membrane Fuel Cell
PV: Photovoltaic

RES: Renewable Energy Sources
SOC: State of Charge
STC: Standard Testing Conditions
WT: wind turbine

7. Notation and symbols

E_{load} : load energy (Wh)
$E_{in,ESS}$: energy stored in the ESS (Wh)
$E_{out,ESS}$: energy discharged by the ESS (Wh)
E_{PV} : photovoltaic energy (Wh)
E_{RES} : RES energy (Wh)
E_{WT} : Wind Turbine energy (Wh)
$LL_\%$: Loss of Load percentage (%)
η_{ESS} : overall storage efficiency
$OP_\%$: Over Production percentage (%)
P_{el}: electrolyser power (W)
$P_{el,\,max}$: maximum electrolyser power (W)
$P_{el,\,nom}$: nominal electrolyser power (W)
P_{fc}: fuel cell power (W)
$P_{fc,\,max}$: maximum fuel cell power (W)
$P_{fc,\,nom}$: nominal fuel cell power (W)
P_{load}: load power (W)
P_{net}: net power (W)
P_{RES}: RES power (W)
p_{tank}: tank pressure (bar)
$p_{tank,0}$: initial tank pressure (bar)
$p_{tank,high}$: high hydrogen tank pressure (bar)
$p_{tank,low}$: low hydrogen tank pressure (bar)
$p_{tank,max}$: maximum hydrogen tank pressure (bar)
$p_{tank,min}$: minimum hydrogen tank pressure (bar)
Q_{batt}: battery capacity (Ah)
Q_{max}: maximum battery capacity (Ah)
SOC_{high}: high State of Charge – restoration (Ah,%)
SOC_{low}: low State of Charge – restoration (Ah,%)
SOC_{max}: maximum State of Charge (Ah,%)
SOC_{min}: minimum State of Charge (Ah,%)
V_{tank} : storage hydrogen tank volume (m^3)

Declaration of Competing Interests

The authors declare that they have no known competing financial interests or personal relationships that could have appeared to influence the work reported in this paper.

Annex I. Electrolyser and Fuel Cell nominal power sensitivity analysis

In this Annex a sensitivity analysis of $P_{el,nom}$ and $P_{fc,nom}$ considering the base-case hydrogen tank volume (V_{tank}=1 m^3=30 Nm^3) is carried out under different EMS. In fact, while V_{tank} determines the energy capacity of the hydrogen ESS, the rate at which P_{net} is converted to H_2 (and viceversa) is strictly dependant from the nominal power of the electrolyser/fuel cell and their dynamic behaviour. From the modelling point of view, a variation of $P_{el,nom}$ and $P_{fc,nom}$ induces a scaling of the current-voltage polarization curves and consequently the maximum power which the electrochemical system is able to process, respect to the P_{net} trend (whose range, as shown in Fig. 9-c, is between −3 kW and +8 kW). The electrolyser nominal power is varied for values equal to 1, 2, 5 and 10 kW$_{e,nom}$, where 10 kW$_{e,nom}$ is the base-case value (currently installed in the microgrid) and maximum value since P_{net} does not exceed 10 kW (Fig. 9-c). The PEMFC nominal power is varied for values equal to 1, 3.3, 6.6 and 10 kW$_{e,nom}$, considering the unit power of each PEMFC system (see Table 2) where 10 kW$_{e,nom}$ is the base-case value considering 3 PEMFC installed in parallel (which is the current configuration of the microgrid). The results of the sensitivity analysis

A. Monforti Ferrario, A. Bartolini, F. Segura Manzano et al.

Advances in Applied Energy 3 (2021) 100048

Table A1.1

H_2-only simulation results (yearly) in function of electrochemical systems' nominal power.
Parameters: V_{tank}=1m^3.

	Variable $P_{el,nom}$ ($P_{fc,nom}$ 10 kW$_e$; V_{tank}=1 m^3)			
	1 kW$_{e,nom}$	2 kW$_{e,nom}$	5 kW$_{e,nom}$	10 kW$_{e,nom}$
E_{el} (MWh)	3.36	4.49	5.07	4.97
E_{fc} (MWh)	1.17	1.56	1.79	1.81
$LL_\%$ (%)	24.74%	17.71%	13.53%	13.22%
$OP_\%$ (%)	60.55%	53.59%	50.05%	50.66%
η_{ESS} (%)	34.25%	34.39%	35.10%	36.14%
	Variable $P_{fc,nom}$ ($P_{el,nom}$ 10 kW$_{e,nom}$; V_{tank}=1 m^3)			
	1 kW$_{e,nom}$	3.3 kW$_{e,nom}$	6.6 kW$_{e,nom}$	10 kW$_{e,nom}$
E_{el} (MWh)	4.50	4.97	4.98	4.97
E_{fc} (MWh)	1.64	1.80	1.81	1.81
$LL_\%$ (%)	16.33%	13.30%	13.27%	13.22%
$OP_\%$ (%)	53.54%	50.57%	50.61%	50.66%
η_{ESS} (%)	36.02%	35.94%	36.02%	36.14%

Table A1.2

Battery-hydrogen (H_2-priority) simulation results (yearly) in function of electrochemical systems' nominal power.
Parameters: Q_{batt}= 100 Ah; V_{tank}=1m^3.

	Var. $P_{el,nom}$ ($P_{fc,nom}$ 10 kW$_e$; V_{tank}=1 m^3; Q_{batt}=100 Ah)			
	1 kW$_{e,nom}$	2 kW$_{e,nom}$	5 kW$_{e,nom}$	10 kW$_{e,nom}$
E_{el} (MWh)	3.36	4.48	5.05	4.96
E_{fc} (MWh)	1.17	1.56	1.79	1.81
$LL_\%$ (%)	23.77%	16.42%	12.29%	12.06%
$OP_\%$ (%)	60.29%	53.26%	49.77%	50.37%
η_{ESS} (%)	35.20%	35.41%	36.00%	36.94%
	Var. $P_{fc,nom}$ ($P_{el,nom}$ 10 kW$_e$; V_{tank}=1 m^3; Q_{batt}=100 Ah)			
	1 kW$_{e,nom}$	3.3 kW$_{e,nom}$	6.6 kW$_{e,nom}$	10 kW$_{e,nom}$
E_{el} (MWh)	4.48	4.97	4.98	4.96
E_{fc} (MWh)	1.63	1.80	1.81	1.81
$LL_\%$ (%)	15.28%	12.20%	12.06%	12.06%
$OP_\%$ (%)	53.32%	50.27%	50.30%	50.37%
η_{ESS} (%)	36.87%	36.67%	36.85%	36.94%

are therefore comparable with the baseline simulation results reported in Table 8.

Although the effect of varying the nominal power of the electrochemical conversion systems is important, the results obtained in this Annex justify the simplificative assumption to neglect the systematic variation of $P_{el,nom}$ and $P_{fc,nom}$ in the optimal design search. Also, given the parametric approach to the optimization process implemented in this study, a complete analysis via parametric analysis all possible combinations of $P_{el,nom}$, $P_{fc,nom}$, Q_{batt} and V_{tank} would be lengthy and cumbersome (2000 possible Q_{batt}/V_{tank} combinations, each of these with 16 possible $P_{el,nom}$/$P_{fc,nom}$ combinations, leading to 32,000 possible scenarios).

A1.1. Single component ESS - H2 only

In Table A1.1 the base-case results of the single-component H_2-only configuration are shown, with a parametric variation of $P_{el,nom}$ and $P_{fc,nom}$. The variation of the electrolyser nominal power shows a greater impact both on the energy processed by the H_2 ESS and on the performance parameters $LL_\%$, $OP_\%$ and η_{ESS} with respect to a variation of the fuel cell nominal power, since if less hydrogen is produced by the electrolyser (upstream component), less hydrogen is available to be consumed by the fuel cell (downstream component) – confirming that the correct sizing of the electrolyser is more critical than correct sizing of the fuel cell.

By increasing $P_{el,nom}$ from 1 kW$_{e,nom}$ to 2 kW$_{e,nom}$, E_{el} and E_{fc} both increase relevantly of around 33%, however a plateau region is reached between 5 kW$_{e,nom}$ and 10 kW$_{e,nom}$, which was expectable due to the maximum value of P_{net}, approximately equal to +8 kW. $LL_\%$ and $OP_\%$ are decreased of around 7%, respectively, while the storage efficiency η_{ESS} is only marginally increased by 0.14%. However, increasing the nominal power in the range 2–10 kW$_{e,nom}$, both the total energy volume processed (10% increase of E_{el} and E_{fc}) and the performance parameters (3–4% reduction of $LL_\%$ and $OP_\%$; 0.15% increase of η_{ESS}) are only slightly affected.

Similarly, increasing $P_{fc,nom}$ from 1 to 3.3 kW$_{e,nom}$ the E_{el} and E_{fc} are only increased by 10% and then remain almost constant with further increase of $P_{fc,nom}$, which was also expectable due to the minimum value of P_{net}, approximately equal to –3 kW. The $LL_\%$ and $OP_\%$ are reduced by 3% in the 1–3.3 kW$_{e,nom}$ range, which is less than half of the impact obtained by varying $P_{el,nom}$, remaining almost constant despite increasing $P_{fc,nom}$ to 10 kW$_{e,nom}$. The variation of η_{ESS} is extremely limited for varying $P_{fc,nom}$ (less than 1%).

A1.2. Hybrid ESS – Battery priority EMS

The effect of $P_{el,nom}$ and $P_{fc,nom}$ under battery-priority EMS is extremely limited due to the small energy volume processed

(<700 kWh/year) by the hydrogen components. No significant effect is produced on both $LL_\%$ and $OP_\%$ by varying both $P_{el,nom}$ and $P_{fc,nom}$ in the range 1-10 kW$_{e,nom}$, unless for very low electrolyser sizes ($P_{el,nom}$ below 1 kW$_{e,nom}$ with a maximum impact on $LL_\%$ below 5%).

A1.3. Hybrid ESS - H2 priority EMS

For the H_2-priority EMS the effect of $P_{el,nom}$ and $P_{fc,nom}$ do affect the main performance parameters LL and OP considering that the H_2 systems prioritization (Table A1.2) induces a larger processed energy volume, although the overall impact is still quite limited, excluding for the 1–2 kW$_{e,nom}$ range.

Similarly to the H_2-only case, by increasing $P_{el,nom}$ from 1 kW$_e$ to 2 kW$_e$ an increase of around 33% is seen in the energy volumes (E_{el} and E_{fc}) with a consequent reduction in $LL_\%$ and $OP_\%$ around 7% and a slight improvement of η_{ESS} of 0.21%. Instead, in the 2–10 kW$_{e,nom}$ range, the impact on the energy volumes is only around 10–14% hence inducinga variation of only 3–4% on the LL% and OP%. The η_{ESS} increases of around 2%, mainly due to moderate current loadings on electrolyser and fuel cell, which contain the voltage losses.

By increasing the $P_{fc,nom}$ from 1 kW$_e$ to 2 kW$_e$ the energy volumes (E_{el} and E_{fc}) are increased by 10%; while $LL_\%$ and $OP_\%$ are only reduced by 3%. In the 2–10 kW$_{e,nom}$ range, both energy volumes and performance parameters are hardly affected (<1%). The storage efficiency η_{ESS} is hardly affected (<0.1%) by the variation of $P_{fc,nom}$ (variation range 36.85–36.94%)

Although the energy processed by the hydrogen ESS is similar to the H_2-only scenario, the hybrid ESS scenario presents a relevant improvement of the performance parameters respect to the H_2-only scenario. The $LL_\%$ in hybrid conditions is in average 1–1.5% lower than in H_2-only conditions; instead the $OP_\%$ improvement of hybridised conditions is limited to around 0.3% respect to the H_2-only scenario. Also with regards of efficiency, the hybrid ESS scenario presents a slight improvement in storage efficiency (around +1% in η_{ESS} in all configurations).

References

[1] International Renewable Energy Agency Global renewables outlook: energy transformation 2050; 2020.

[2] Bailera M, Peña B, Lisbona P, Romeo LM. Decision-making methodology for managing photovoltaic surplus electricity through Power to Gas: combined heat and power in urban buildings. Appl Energy 2018;228:1032–45. doi:10.1016/j.apenergy.2018.06.128.

[3] Zerrahn A, Schill W, Kemfert C. On the economics of electrical storage for variable renewable energy sources. Eur Econ Rev 2018;108:259–79. doi:10.1016/j.euroecorev.2018.07.004.

[4] IPCC Summary for policymakers - Global warming of 1.5°C, an IPCC special report; 2018.

[5] IRENA Renewable energy integration in power grids. Technology brief; 2015.

[6] Eriksson ELV, Gray EMA. Optimization and integration of hybrid renewable energy hydrogen fuel cell energy systems – a critical review. Appl Energy 2017;202:348–64. doi:10.1016/j.apenergy.2017.03.132.

[7] Eriksson ELV, Gray EMA. Optimization of renewable hybrid energy systems – A multi-objective approach. Renew Energy 2019;133:971–99. doi:10.1016/j.renene.2018.10.053.

[8] Hernández JC, Sanchez-Sutil F, Muñoz-Rodríguez FJ. Design criteria for the optimal sizing of a hybrid energy storage system in PV household-prosumers to maximize self-consumption and self-sufficiency. Energy 2019;186. doi:10.1016/j.energy.2019.07.157.

[9] Dunn B., Kamath H., Tarascon J. Electrical energy storage for the grid: a battery of choices 2011;334:928–36.

[10] Department of Energy DOE, Mongird K, Viswanathan V, Balducci P, Alam J, Fotedar V, et al. Energy Storage Technology and Cost Characterization Report; 2019.

[11] ISEA. Technology Overview on Electricity Storage 2012.

[12] Nastasi B, Lo Basso G, Astiaso Garcia D, Cumo F, de Santoli L. Power-to-gas leverage effect on power-to-heat application for urban renewable thermal energy systems. Int J Hydrogen Energy 2018;43:23076–90. doi:10.1016/j.ijhydene.2018.08.119.

[13] IEA International Energy Agency The future of fuel: the future of hydrogen. report; 2019. doi:10.1016/S1464-2859(12)70027-5.

[14] Dagdougui H., Sacile R., Bersani C., Ouammi A. Hydrogen Storage and Distribution: implementation Scenarios 2018;37–52. doi:10.1016/B978-0-12-812036-1.00004-4.

[15] Murray P, Orehounig K, Grosspietsch D, Carmeliet J. A comparison of storage systems in neighbourhood decentralized energy system applications from 2015 to 2050. Appl Energy 2018;231:1285–306. doi:10.1016/j.apenergy.2018.08.106.

[16] Milo A, Gaztañaga H, Etxeberria-otadui I, Bacha S, Rodríguez P. Optimal economic exploitation of hydrogen based grid-friendly zero energy buildings. Renew Energy 2011;36:197–205. doi:10.1016/j.renene.2010.06.021.

[17] Semaoui S, Hadj Arab A, Bacha S, Azoui B. The new strategy of energy management for a photovoltaic system without extra intended for remote-housing. Sol Energy 2013;94:71–85. doi:10.1016/j.solener.2013.04.029.

[18] Gomez-Gonzalez M, Hernandez JC, Vera D, Jurado F. Optimal sizing and power schedule in PV household-prosumers for improving PV self-consumption and providing frequency containment reserve. Energy 2020;191:116554. doi:10.1016/j.energy.2019.116554.

[19] Eurostat. Energy consumption in households; 2020. https://ec.europa.eu/eurostat/statistics-explained/index.php/Energy_consumption_in_households#Energy_consumption_in_households_by_type_of_end-use. p. 3–9.

[20] Bartolini A, Carducci F, Muñoz CB, Comodi G. Energy storage and multi energy systems in local energy communities with high renewable energy penetration. Renew Energy 2020;159:595–609. doi:10.1016/j.renene.2020.05.131.

[21] Baumann L, Boggasch E, Rylatt M, Wright A. Energy flow management of a hybrid renewable energy system with hydrogen. In: IEEE Conf. Innov. Technol. an Effic. Reliab. Electr. Supply; 2010. p. 78–85. doi:10.1109/CITRES.2010.5619856.

[22] Hosseinalizadeh R, Shakouri GH, Sadegh M, Taghipour P. Economic sizing of a hybrid (PV – WT – FC) renewable energy system (HRES) for stand-alone usages by an optimization-simulation model: case study of Iran. Renew Sustain Energy Rev 2016;54:139–50. doi:10.1016/j.rser.2015.09.046.

[23] Erdinc O., Uzunoglu M. Optimum design of hybrid renewable energy systems: overview of different approaches 2012;16:1412–25. doi:10.1016/j.rser.2011.11.011.

[24] Abdin Z, Webb CJ, Gray EM. Solar hydrogen hybrid energy systems for off-grid electricity supply: a critical review. Renew Sustain Energy Rev 2015;52:1791–808. doi:10.1016/j.rser.2015.08.011.

[25] Gangwar S, Bhanja D, Biswas A. Cost, reliability, and sensitivity of a stand-alone hybrid renewable energy system—A case study on a lecture building with low load factor. J Renew Sustain Energy 2015:013109. doi:10.1063/1.4906916.

[26] Eltamaly AM, Mohamed MA, Abdulrahman I. Load management as a smart grid concept for sizing and designing of hybrid renewable energy systems. Eng Optim 2017;49:1813–28. doi:10.1080/0305215X.2016.1261246.

[27] Li B, Roche R, Paire D, Miraoui A. Sizing of a stand-alone microgrid considering electric power, cooling/heating, hydrogen loads and hydrogen storage degradation. Appl Energy 2017;205:1244–59. doi:10.1016/j.apenergy.2017.08.142.

[28] Li B, Roche R, Miraoui A. Microgrid sizing with combined evolutionary algorithm and MILP unit commitment. Appl Energy 2017;188:547–62. doi:10.1016/j.apenergy.2016.12.038.

[29] Castañeda M, Cano A, Jurado F, Sánchez H, Fernández LM. Sizing optimization, dynamic modeling and energy management strategies of a stand-alone PV/hydrogen/battery-based hybrid system. Int J Hydrogen Energy 2013;38:3830–45. doi:10.1016/j.ijhydene.2013.01.080.

[30] Bartolucci L, Cordiner S, Mulone V, Pasquale S. Fuel cell based hybrid renewable energy systems for off-grid telecom stations: data analysis and system optimization. Appl Energy 2019;252:113386. doi:10.1016/j.apenergy.2019.113386.

[31] Cau G, Cocco D, Petrollese M, Tola V. Assessment of a Hybrid Stand-Alone Power System with Hydrogen Production and Storage. 3rd Int. Conf. Microgeneration Relat. Technol.; 2013.

[32] Kaviani AK, Riahy GH, Kouhsari SHM. Optimal design of a reliable hydrogen-based stand-alone wind /PV generating system, considering component outages. Renew Energy 2009;34:2380–90. doi:10.1016/j.renene.2009.03.020.

[33] Monforti Ferrario A, Vivas FJ, Segura Manzano F, Andujar JM, Bocci E, Martirano L. Hydrogen vs. Battery in the Long-term Operation. A Comparative Between Energy Management Strategies for Hybrid Renewable Microgrids. Electronics (Basel) 2020;9:1–27.

[34] Vivas FJ, Segura F, Andújar JM, Caparrós JJ. A suitable state-space model for renewable source-based microgrids with hydrogen as backup for the de-

[35] Vivas FJ, De las Heras A, Segura F, Andújar JM. H2RES2 simulator. A new solution for hydrogen hybridization with renewable energy sources-based systems. Int J Hydrogen Energy 2017;42:13510–31. doi:10.1016/j.ijhydene.2017.02.139.

[36] Kavadias KA, Apostolou D, Kaldellis JK. Modelling and optimisation of a hydrogen-based energy storage system in an autonomous electrical network. Appl Energy 2018;227:574–86. doi:10.1016/j.apenergy.2017.08.050.

[37] Hafez O, Bhattacharya K. Optimal planning and design of a renewable energy based supply system for microgrids. Renew Energy 2012;45:7–15. doi:10.1016/j.renene.2012.01.087.

[38] Serra F, Lucariello M, Petrollese M, Cau G. Optimal integration of hydrogen-based energy storage systems in photovoltaic microgrids: a techno-economic assessment; 2020.

[39] N Mat Isa, H Shekhar Das, C Wei Tan, Yatim AHM, Yiew Lau K. A techno-economic assessment of a combined heat and power photovoltaic /fuel cell / battery energy system in Malaysia hospital. Energy 2016;112:75–90. doi:10.1016/j.energy.2016.06.056.

[40] Mostofi F, Shayeghi H. Feasibility and Optimal Reliable Design of Renewable Hybrid Energy System for Rural Electrification in Iran. Int J Renew Energy Res 2012;2.

[41] Valverde L, Rosa F, Del Real AJ, Arce A, Bordons C. Modeling, simulation and experimental set-up of a renewable hydrogen-based domestic microgrid. Int J Hydrogen Energy 2013;38:11672–84. doi:10.1016/j.ijhydene.2013.06.113.

[42] Bruni G, Cordiner S, Galeotti M, Mulone V, Nobile M, Rocco V. Control Strategy Influence on the Efficiency of a Hybrid Photovoltaic-Battery-Fuel Cell System Distributed Generation System for Domestic Applications. Energy Procedia 2014;45:237–46. doi:10.1016/j.egypro.2014.01.026.

[43] Voutetakis S, Stergiopoulos F, Seferlis P, Ipsakis D, Ziogou C, Papadopoulos A, et al. Design of a Stand-Alone Power System using Renewable Energy Sources and Long-Term Hydrogen Storage Handb. Sustain. Energy Lee WH, Cho GV, editors. Nova Science Publishers Inc; 2021. n.d.

[44] Dash V, Bajpai P. Power management control strategy for a stand-alone solar photovoltaic-fuel cell-battery hybrid system. Sustain Energy Technol Assessments 2015;9:68–80. doi:10.1016/j.seta.2014.10.001.

[45] Terlouw T, AlSkaif T, Bauer C, van Sark W. Optimal energy management in all-electric residential energy systems with heat and electricity storage. Appl Energy 2019;254:113580. doi:10.1016/j.apenergy.2019.113580.

[46] Cau G, Cocco D, Petrollese M, Knudsen Kær S, Milan C. Energy management strategy based on short-term generation scheduling for a renewable microgrid using a hydrogen storage system. Energy Convers Manag 2014;87:820–31. doi:10.1016/j.enconman.2014.07.078.

[47] Erdinc O, Uzunoglu M. The importance of detailed data utilization on the performance evaluation of a grid-independent hybrid renewable energy system. Int J Hydrogen Energy 2011;36:12664–77. doi:10.1016/j.ijhydene.2011.07.060.

[48] Zeugmann T. Particle swarm optimization. In: Encycl. Mach. Learn., vol. 780. © Springer Science+Business Media; 2011. p. 746–817. doi:10.1007/978-3-319-93025-1_2.

[49] JRC European Commission. JRC Photovoltaic Geographical Information System (PVGIS) 2019. https://re.jrc.ec.europa.eu/pvg_tools/en/tools.html#TMY.

[50] Cebecauer T, Suri M. Typical Meteorological Year Data: solarGIS Approach Typical Meteorological Year data: solarGIS approach. Energy Procedia 2016;69:1958–69. doi:10.1016/j.egypro.2015.03.195.

[51] Mousavi Maleki SA, Hizam H, Gomes C. Estimation of hourly, daily and monthly global solar radiation on inclined surfaces: models re-visited. Energies 2017;10:1–28. doi:10.3390/en10010134.

[52] Bañuelos-ruedas F, Camacho CÁ. Methodologies used in the extrapolation of wind speed data at different heights and its impact in the wind energy resource assessment in a region. In: Wind Farm - Tech. Regul. Potential Estim. Siting Assess.. InTech; 2011. p. 98–134.

[53] Melgar Sergio Gómez Martínez, Bohórquez MÁ. Andújar Márquez JM. uhuMEBr: energy Refurbishment of Existing Minimum Energy Buildings. Energies 2020; 13:1–35.

[54] Comodi G, Cioccolanti L, Renzi M. Modelling the Italian household sector at the municipal scale: micro-CHP, renewables and energy efficiency. Energy 2014;68:92–103. doi:10.1016/j.energy.2014.02.055.

[55] Escobar P, Martínez E, Saenz-Díez JC, Jiménez E, Blanco J. Modeling and analysis of the electricity consumption profile of the residential sector in Spain. Energy Build 2020;207:109629. doi:10.1016/j.enbuild.2019.109629.

[56] Monforti Ferrario A., Amoruso C., Robles R.V., Del Zotto L., Bocci E., Comodi G. Power-to-Gas from curtailed RES electricity in Spain: potential and applications 2020;1–6. doi:10.1109/eeeic/icpseurope49358.2020.9160820.

[57] Official Journal of the European Union. Directive 2010/31/EU of the European Parliament and of the Council of 19 May 2010 on the energy performance of buildings (recast). 2010.

[58] Camps X, Velasco G, de la Hoz J, Martín H. Contribution to the PV-to-inverter sizing ratio determination using a custom flexible experimental setup. Appl Energy 2015;149:35–45. doi:10.1016/j.apenergy.2015.03.050.

[59] Feroldi D, Degliuomini LN, Basualdo M. Energy management of a hybrid system based on wind-solar power sources and bioethanol. Chem Eng Res Des 2013;91:1440–55. doi:10.1016/j.cherd.2013.03.007.

[60] Ulleberg Ø. Modeling of advanced alkaline electrolyzers: a system simulation approach. Int J Hydrogen Energy 2003;28:21–33. doi:10.1016/S0360-3199(02)00033-2.

[61] Tremblay O, Dessaint LA. Experimental validation of a battery dynamic model for EV applications. World Electr Veh J 2009;3:289–98.

[62] Vivas F.J., Heras A., Segura F., Andujar J.M. Cell voltage monitoring All-in-One . A new low cost solution to perform degradation analysis on air- cooled polymer electrolyte fuel cells 2018;4. doi:10.1016/j.ijhydene.2018.12.172.

[63] EERA European Energy Research Alliance. Key performance indicators (KPIs) for FCH research and innovation, 2020 - 2030; 2020. p. 2020–30.

[64] Fan L, Zhang G, Jiao K. Characteristics of PEMFC operating at high current density with low external humidification. Energy Convers Manag 2017;150:763–74. doi:10.1016/j.enconman.2017.08.034.

[65] Marangio F, Santarelli M, Calì M. Theoretical model and experimental analysis of a high pressure PEM water electrolyser for hydrogen production. Int J Hydrogen Energy 2009;34:1143–58. doi:10.1016/j.ijhydene.2008.11.083.

[66] Nikmehr N, Najafi-Ravadanegh S, Khodaei A. Probabilistic optimal scheduling of networked microgrids considering time-based demand response programs under un-certainty. Appl Energy 2017;198:267–79. doi:10.1016/j.apenergy.2017.04.071.

[67] Layadi TM, Champenois G, Mostefai M, Abbes D. Lifetime estimation tool of lead-acid batteries for hybrid power sources design. Simul Model Pract Theory 2015;54:36–48. doi:10.1016/j.simpat.2015.03.001.

[68] Ipsakis D, Voutetakis S, Seferlis P, Stergiopoulos F, Papadopoulou S, Elmasides C. The effect of the hysteresis band on power management strategies in a stand-alone power system. Energy 2008;33:1537–50. doi:10.1016/j.energy.2008.07.012.

[69] Al-Sharafi A, Sahin AZ, Ayar T, Yilbas BS. Techno-economic analysis and op-timization of solar and wind energy systems for power generation and hy-drogen production in Saudi Arabia. Renew Sustain Energy Rev 2017;69:33–49. doi:10.1016/j.rser.2016.11.157.

[70] Shivakumar A, Welsch M, Taliotis C, Jakšić D, Baričević T, Howells M, et al. Valuing blackouts and lost leisure: estimating electricity interruption costs for households across the European Union. Energy Res Soc Sci 2017;34:39–48. doi:10.1016/j.erss.2017.05.010.

[71] Schröder T, Kuckshinrichs W. Value of lost load: an efficient economic indicator for power supply security? A literature review. Front Energy Res 2015;3:1–12. doi:10.3389/fenrg.2015.00055.

[72] Steilen M, Jörissen L. Hydrogen Conversion into Electricity and Thermal Energy by Fuel Cells: use of H2-Systems and Batteries. Electrochem Energy Storage Renew Sources Grid Balanc 2015:143–58. doi:10.1016/B978-0-444-62616-5.00010-3.

[73] Reuß M, Grube T, Robinius M, Preuster P, Wasserscheid P, Stolten D. Seasonal stor-age and alternative carriers: a flexible hydrogen supply chain model. Appl Energy 2017;200:290–302. doi:10.1016/j.apenergy.2017.05.050.

[74] IRENA Electricity storage and renewables: costs and markets to 2030; 2017.

[75] MathWorks. Particle swarm optimization - MATLAB particleswarm; 2021. https://it.mathworks.com/help/gads/particleswarm.html (accessed April 30, 2021) p. 1–8.

[76] García P, Torreglosa JP, Fernández LM, Jurado F. Optimal energy manage-ment system for stand-alone wind turbine/photovoltaic/hydrogen/battery hybrid system with supervisory control based on fuzzy logic. Int J Hydrogen Energy 2013;38:14146–58. doi:10.1016/j.ijhydene.2013.08.106.

[77] Rozzi M, Mascherpa M, Grimaccia F, Leva S. Hybrid renewable power system for radio networks in mission critical applications; 2020.

[78] Achaibou N, Haddadi M, Malek A. Modeling of lead acid batteries in PV systems. Energy Procedia 2012;18:538–44. doi:10.1016/j.egypro.2012.05.065.

[79] Fioriti D, Lutzemberger G, Poli D, Duenas-martinez P, Micangeli A. Heuristic ap-proaches to size microgrids: a methodology to compile multiple design options; 2020.

[80] Ulleberg Ø, Nakken T, Eté A. The wind/hydrogen demonstration system at Utsira in Norway: evaluation of system performance using operational data and updated hydrogen energy system modeling tools. Int J Hydrogen Energy 2010;35:1841–52. doi:10.1016/j.ijhydene.2009.10.077.